Available online at website: https://journal.bcrec.id/index.php/jcerp

Journal of Chemical Engineering Research Progress, 3 (2) 2026, 369-389

Original Research Article

Acacia auriculiformis-Derived Cellulose Nanoparticles as a Sustainable Nanofluid for Enhanced Oil Recovery

Francis Nyah[1*], David Abutu[1], Kufre Mkpadem[2], Money Barima[1], Okorie Agwu[3,4], Norida Ridzuan[1*]

[1]*Faculty of Chemical and Process Engineering Technology, Universiti Malaysia Pahang Al-Sultan Abdullah, Lebuhraya Persiaran Tun Khalil Yaakob 26300 Kuantan, Pahang, Malaysia, Gambang, Pahang, Malaysia.*

[2]*School of Computing and Digital Studies, Sheffield Hallam University, Sheffield, England, United Kingdom.*

[3]*Petroleum Engineering Department, University Teknologi PETRONAS, 32610, Seri Iskandar, Perak Darul Ridzuan, Malaysia.*

[4]*Center of Reservoir Dynamics (CORED), Institute of Sustainable Energy, Universiti Teknologi, PETRONAS, 32610, Seri Iskandar, Perak Darul Ridzuan, Malaysia.*

Received: 12th August 2026; Revised: 3rd September 2026; Accepted: 5th September 2026
Available online: 8th September 2026; Published regularly: December 2026

Abstract

Conventional enhanced oil recovery (EOR) methods often lose effectiveness under high-temperature, high-salinity (HTHS) conditions because of inadequate fluid stability, limited wettability alteration, and insufficient interfacial tension (IFT) reduction. This study developed and evaluated cellulose nanoparticles (CNPs) derived from Acacia auriculiformis as a sustainable nanofluid for EOR. CNPs were extracted using a deep eutectic solvent (DES) process and surface-modified to improve thermal stability and interfacial functionality. Structural, morphological, compositional, and thermal characteristics were evaluated, while the resulting cellulose nanofluid (CNF) was assessed through rheology, IFT, contact-angle, and sand-pack flooding experiments. The process yielded 78.3% CNP, with an average particle size of 19.65 ± 0.2 nm and crystallinity index (CrI) of 76.6%, confirming successful formation of crystalline nanocellulose. At 0.2 wt%, CNF reduced oil-water IFT to approximately 7.8 mN/m at elevated temperature and decreased the sandstone contact angle to 16.5°, indicating strong water-wet alteration. Sand-pack flooding achieved 13.7% incremental oil recovery and 72.3% total recovery, compared with 9.8% incremental recovery and 63.1% total recovery for xanthan. The superior performance is attributed to the combined effects of IFT reduction, wettability alteration, mobility control, and thermal stability. Overall, Acacia-derived CNF demonstrates greater EOR potential than xanthan and represents a promising, environmentally sustainable nanofluid for challenging reservoir conditions.

Keywords: Interfacial tension; xanthan; cellulose nanofluid; contact angle; Enhanced oil recovery; Acacia auriculiformis

How to Cite: Nyah, F., David, A., Mkpadem, K., Barima, M., Agwu, O., Ridzuan, N. (2026) Acacia auriculiformis-Derived Cellulose Nanoparticles as a Sustainable Nanofluid for Enhanced Oil Recovery. *Journal of Chemical Engineering Research Progress*, 3 (2), 369-389 (DOI: 10.9767/jcerp.20816)

Permalink/DOI: https://doi.org/10.9767/jcerp.20816

1. Introduction

Global energy insecurity, geopolitical disruptions, and the transition toward lower-carbon energy systems continue to sustain the importance of crude oil within the global energy portfolio [1,2]. Consequently, enhanced oil recovery (EOR) remains important for mobilizing residual oil trapped after primary and secondary recovery. Following water or gas flooding, a substantial fraction of the Original Oil in Place (OOIP) remains unrecovered because of capillary forces, high oil-water IFT, unfavorable wettability, and reservoir heterogeneity. Chemical enhanced oil recovery (CEOR), including polymer, surfactant, alkaline, and foam flooding, has therefore attracted considerable attention because of its ability to improve oil displacement and sweep efficiency at relatively low cost and with

* Corresponding Author.
Email: rancis.nyah@yahoo.com (F. Nyah);
norida@umpsa.edu.my (N. Ridzuan).

established operational practices [3,4]. Sweep efficiency is the fraction of a reservoir volume effectively contacted by an injected fluid during secondary or enhanced oil recovery. It describes how well the injected fluid reaches oil-bearing regions rather than bypassing them. Sweep efficiency comprises areal sweep, which represents horizontal reservoir coverage, and vertical sweep, which reflects fluid penetration through reservoir layers. High sweep efficiency indicates uniform fluid distribution and greater reservoir contact, whereas low sweep efficiency results from channeling through high-permeability zones or fractures, leaving oil unswept. Therefore, improving sweep efficiency is essential for maximizing oil recovery.

Among CEOR agents, hydrolyzed polyacrylamide (HPAM) is widely used for mobility control because its incorporation into the aqueous phase increases viscosity and reduces the mobility ratio between injected water and oil [5]. This suppresses viscous fingering and premature water breakthrough while improving displacement-front stability. HPAM can also increase flow resistance in high-permeability zones, diverting the injected fluid toward less-swept regions and consequently improving macroscopic sweep efficiency [6]. Nevertheless, conventional CEOR systems can experience viscosity loss, thermal degradation, precipitation, and deterioration of interfacial performance under HTHS reservoir conditions [7,8].

Similarly, under HTHS conditions, conventional CEOR fluids such as HPAM and surfactants suffer reduced performance. High temperature accelerates HPAM hydrolysis and backbone degradation, while Na^+ shields electrostatic repulsion, causing polymer chains to coil, reducing hydrodynamic volume and viscosity [9]. Ca^{2+} and Mg^{2+} can bridge negatively charged HPAM chains, causing aggregation and precipitation that may impair injectivity [10]. Meanwhile, high salinity and temperature alter surfactant hydration, micellar structure, phase behaviour, and hydrophilic-lipophilic balance, increasing adsorption and reducing IFT-reduction and wettability-alteration efficiency. Consequently, HTHS conditions compromise polymer mobility control, fluid stability, injectivity, and interfacial performance, ultimately reducing CEOR effectiveness. These limitations have stimulated interest in nanoparticle-assisted EOR.

Nanoparticle-assisted EOR has consequently emerged as a promising strategy because nanoparticles possess a high specific surface area, thermal stability, and potential resistance to salinity-induced degradation. Their interactions with rock surfaces and reservoir fluids can promote wettability alteration, IFT reduction, rheological modification, asphaltene stabilization, and mobility control [11-13]. For example, Al_2O_3 nanoparticles have been reported to improve the thermal resistance of HPAM through a shielding effect, whereas SiO_2 and graphene oxide can enhance polymer tolerance to elevated salinity and temperature [14,15]. Nevertheless, prolonged exposure to harsh reservoir conditions may weaken nanoparticle-polymer interactions through bond degradation, particle aggregation, and changes in surface chemistry, thereby compromising long-term performance [16,17]. The development of intrinsically robust, salt-tolerant, and thermally stable nanomaterials is therefore essential for maintaining nanoparticle functionality throughout the EOR process. In this regard, the effectiveness of nanoparticles is closely associated with their interfacial behaviour and their ability to interact with both reservoir fluids and mineral surfaces [18].

These interfacial interactions enable nanoparticles to improve colloidal stability, wettability, and IFT. Their high specific surface area promotes adsorption at oil-water or gas-liquid interfaces, forming protective layers that inhibit droplet coalescence and film rupture, thereby enhancing emulsion and foam stability [19]. At solid-fluid interfaces, nanoparticle adsorption modifies surface charge, hydration, and surface free energy, facilitating oil displacement and shifting rock wettability from oil-wet toward water-wet conditions [20,21]. Similarly, nanoparticle accumulation at oil-water interfaces can reduce interfacial free energy and IFT, improving oil displacement and multiphase-flow control [22]. These effects highlight the importance of nanoparticle surface chemistry, adsorption, dispersion, and thermal stability under reservoir conditions.

The high specific surface area of nanoparticles provides abundant active sites for interactions with polymers, surfactants, and dissolved ions, thereby contributing to improved thermal stability and salinity tolerance [23]. Under elevated temperatures, nanoparticle-polymer interactions can restrict chain degradation and preserve rheological properties, while surface functional groups can mitigate ion-induced polymer contraction, aggregation, and precipitation in saline brines [24]. These effects depend on key nanoparticle characteristics, including specific surface area, thermally stable cores, surface charge, functional groups, interaction strength, and steric stabilization. These properties help maintain nanoparticle dispersion, polymer conformation, viscosity, and interfacial functionality under HTHS conditions, although their effectiveness depends on particle composition, size, concentration, surface

modification, and compatibility with the polymer and brine chemistry [25,26]. Consequently, beyond improving nanoparticle performance, increasing attention has been directed toward the development of sustainable nanomaterials that can provide these interfacial functions while reducing environmental and economic concerns associated with conventional inorganic nanomaterials.

Biomass-derived nanomaterials offer an attractive alternative because of their abundance, renewability, biodegradability, low cost, and tunable physicochemical properties [27,28]. Lignocellulosic biomass can produce cellulose nanocrystals (CNCs), biochars, and graphene-like materials. Acacia-derived nanomaterials have previously demonstrated promising performance in adsorption and photocatalytic degradation, highlighting the potential of Acacia biomass as a versatile precursor for functional nanomaterials [29]. These characteristics provide a basis for exploring Acacia-derived cellulose nanomaterials as functional additives for nanofluid-based enhanced oil recovery. Nguyen *et al.* [30] demonstrated strong relationships between Acacia-derived biochar properties and adsorption performance. Mary *et al.* [31] further achieved 93% methylene-blue degradation using Acacia-derived eco-graphite/rGO-MoO_3 photocatalysts.

Despite these advances, Acacia-derived nanomaterials remain largely unexplored for EOR. In particular, the capability of CNP derived from *Acacia auriculiformis* to withstand HTHS conditions while improving wettability, IFT, rheology, and oil displacement remains insufficiently understood. Moreover, existing approaches predominantly modify conventional polymers and surfactants rather than developing inherently robust biomass-derived CEOR materials. Accordingly, this study aims to extract cellulose from *A. auriculiformis* bark, convert it into surface-modified CNP, and evaluate their physicochemical, structural, interfacial, rheological, and oil-recovery performance under reservoir-relevant conditions. The novelty lies in introducing *A. auriculiformis* bark as a sustainable precursor for cellulose-based nanomaterials specifically designed for CEOR. The bark contains five triterpenoid saponins, proacaciaside-I, proacaciaside-II, acaciamine, acaciasides A and B, with structural characteristics that may enhance interfacial activity [23]. Unlike previous Acacia applications in remediation, this study investigates wettability alteration, IFT reduction, rheological enhancement, and structural disjoining pressure for oil displacement. The work therefore bridges biomass valorization, nanotechnology, and petroleum engineering, while advancing sustainable CEOR alternatives and supporting a circular bioeconomy. To achieve these objectives, DESs were considered particularly relevant because their tunable physicochemical and interfacial properties could facilitate both biomass fractionation and subsequent nanomaterial functionalization.

DESs possess distinctive physicochemical properties arising from strong hydrogen-bonding and ion-dipole interactions between hydrogen-bond acceptors (HBAs) and hydrogen-bond donors (HBDs) [32,33]. These interactions can modify solvent polarity, activity, viscosity, and solvation behaviour, making DESs effective media for biomass processing and material modification. During cellulose extraction, the extensive hydrogen-bonding interactions of DESs can facilitate the disruption of lignocellulosic structures and promote the selective dissolution or removal of lignin and hemicellulose, thereby increasing cellulose accessibility and recovery [34]. Their relatively low vapour pressure, tunable polarity, and adjustable viscosity can further influence solvent penetration and mass transfer within the biomass matrix. In addition, the relatively high density of many DES formulations, typically within 1.0 - 1.4 g/cm^3, can affect phase behaviour and solute-solvent interactions [35]. These characteristics make DESs attractive alternatives to conventional organic solvents for the sustainable extraction and preparation of cellulose-based nanomaterials.

Beyond their role in biomass fractionation, DESs can also influence the colloidal stability and interfacial functionality of the resulting nanomaterials. Extensive hydrogen-bonding and ion-dipole interactions can modify surface chemistry and molecular organization, while preferential interactions with solid or polymer surfaces can alter surface energy, hydration, and wettability [36]. DES treatment can also disrupt hydrogen-bond networks within cellulose, increasing the accessibility of hydroxyl and other polar functional groups that can participate in subsequent surface modification [37]. Such interactions provide opportunities for one-pot functionalization processes, including esterification, grafting, and plasticization, enabling controlled adjustment of nanoparticle surface properties. Consequently, the combined extraction and functionalization capabilities of DESs provide a rational basis for producing surface-modified CNPs with improved dispersion and interfacial activity, which are essential characteristics for their application in CEOR under demanding reservoir conditions.

2. Materials and Methods

2.1. Materials

Acacia auriculiformis bark was collected from the Gambang Campus of Universiti Malaysia Pahang Al-Sultan Abdullah (UMPSA). Choline chloride (98%), citric acid monohydrate (98%), hydrogen peroxide (35%), sodium hypochlorite, ethanol (95%; CAS 64-17-6), sodium chloride, sodium hydroxide, and acetic acid (5%; density 1.0446 g/cm^3 at 25 °C) were commercially obtained and used without further purification. Sarawak crude oil had a density of 0.874 g/mL, API gravity of 36.2°, and viscosity of 9.67 cP at 25 °C. Sarawak sandstone cores were used, with properties listed in Table 1. (The reported parameters correspond to the complete sand-pack sample used in each experiment, unless otherwise stated). For typical sand-pack EOR experiments, parameters such as sand mass, bulk volume, pore volume, porosity, permeability, and initial oil saturation are generally characteristics of the whole sand pack, not "per gram". Water specifications and crude-oil properties are provided in Table 2.

Table 1. Physical and petrophysical characteristics of the sand-pack samples used in the core-flooding experiments (H_2O/CO_2 on 13X/Y).

Properties	Core
Length (cm)	9.5
Diameter (cm)	3.5
Bulk volume (cm^3)	104.4
Pore volume (cm^3)	29.7
Porosity (%)	28.4.2
Permeability (mD)	152.24
Initial oil saturation (%)	93.44
Injection rate (mL/min)	0.5

2.2. Preparation of Acacia auriculiformis Bark

Acacia auriculiformis bark was washed sequentially with tap and distilled water to remove impurities. It was air-dried for 5-7 days and subsequently oven-dried at 75 °C for 24 h to achieve constant weight. The dried bark was ground using a laboratory grinder and sieved through a 250 µm mesh to obtain uniform particles. The processed powder was stored in sealed containers for subsequent cellulose extraction and nanoparticle synthesis. The preparation procedure is presented in Figure 1.

Table 2. Physiochemical properties of crude oil.

Physical Properties	Value
Viscosity (cP)	9.67
Density (g/cm^3)	0.874
Specific gravity	0.874
API Gravity (^{o}API)	36.2

Figure 1. Sequence of Acacia bark preparation.

2.3. Acacia Bark Pretreatment

Dried *Acacia auriculiformis* bark was delignified with 5% aqueous NaOH at a 1:20 solid-to-liquid ratio (g/mL) for 2 h. The treated material was washed with distilled water to neutral pH and oven-dried at 60 °C to constant weight. It was subsequently bleached using 3 wt% NaClO at a 1:20 pulp-to-liquid ratio for 1 h, washed to neutral pH, and dried at 60 °C. Cellulose yield (Y, %) was calculated using Equation (1).

$$EY(\%) = \frac{W_C}{W_{pw}} \times 100\% \quad (1)$$

whereas W_{pw} and W_c are the masses (g) of the initial raw paper wastes and extracted cellulose, respectively.

2.4. DES Solvent Preparation

Choline chloride (ChCl) and citric acid (CA) were selected as DES components based on their demonstrated suitability for cellulose fractionation. The DES was prepared by mixing ChCl and CA at a 1:1 molar ratio for 1 h at 70 °C under continuous magnetic stirring until a homogeneous solution was obtained [38].

2.5. Hydrolysis of Bleached Acacia Pulp via DES

The DES was formulated using choline chloride (ChCl) as the hydrogen bond acceptor (HBA) and citric acid monohydrate (CA) as the hydrogen bond donor (HBD) at a 1:2 molar ratio. Their molecular weights were 139.62 and 210.14 g.mol^{-1}, respectively, giving a combined molar mass of 349.76 g.mol^{-1}. Therefore, to prepare a 200 mL DES solution, these calculations were done:

Total DES = Mol. wt. of ChCl +Mol. wt. of CA (2)

$$Mass\ fraction\ of\ ChCl = \frac{Molecular\ of\ ChCl}{Total\ DES} \times 100\% \quad (3)$$

The calculated masses ensured accurate ChCl-CA formulation. The components were stirred at 80 °C until a clear homogeneous DES formed, cooled, and stored in a sealed glass container to minimize moisture uptake [41]. DIW (40 mL) was gradually incorporated under gentle stirring, followed by A. auriculiformis pulp at a 1:10 pulp-to-solvent ratio (20 g pulp/200 mL DES). The suspension was maintained at 100 °C for 4 h to selectively remove lignin and hemicellulose, while preserving cellulose. Treatment temperature, time, water content, and biomass loading were varied. The product was diluted tenfold, filtered, repeatedly washed with water and ethanol to neutral pH, dried at 60 °C, and stored airtight. Yield was determined using Equation (4) [39].

$$Y(\%) = \frac{W_{CNP}}{W_C} \times 100\% \quad (4)$$

whereas W_C and W_{CNP} are the masses (g) of the initial raw paper wastes and extracted cellulose after DES treatment, respectively.

2.6. Characterization of Cellulose and CNPs

2.6.1. Determination of functional groups via FTIR

Functional groups in bleached Acacia auriculiformis pulp and DES-treated CNPs were analyzed using a Spectrum 65 FTIR spectrometer (PerkinElmer). Each 1 mg sample was mixed with 100 mg KBr, pelletized at 80 kN for 2 min, and scanned from 4000-450 cm^{-1} using 16 scans. Spectrum was smooth and baseline-corrected with PerkinElmer Spectrum software.

2.6.2. XRD

The crystallographic characteristics of bleached pulp cellulose and DES-treated cellulose nanocrystals (CNPs) were evaluated using a SmartLab high-resolution X-ray diffractometer with a HyPix-3000 detector. Measurements employed Bragg–Brentano geometry over 2θ = 2°–40°, with a 0.01° step and 1°.min^{-1} scan rate, at 45 kV and 200 mA [40]. The crystallinity index (CrI) was calculated using Equation (5).

$$CrI\% = \frac{I_{200} - I_{am}}{I_{200}} \times 100\% \quad (5)$$

whereas CrI% is the measured apparent crystallinity, I_{200} is the intensity of the 200 peak and I_{am} is the contribution from the amorphous cellulose taken at the minimum between the 110 and 200 peaks.

2.6.3. Thermal analysis (TGA/DTG)

The sample's thermal stability was investigated using Mettler Toledo, TGA/DSC 3+. The material was initially dried at a rate of 10 °C per minute before being heated to 900 °C in a nitrogen atmosphere.

2.6.4. SEM/FESEM

The morphology of bleached Acacia auriculiformis pulp and DES-treated CNPs was examined using JSM-7001F and LEO SUPRA 50VP FESEM systems. Samples were mounted on aluminum stubs using conductive carbon tape and sputter-coated with platinum using a JEOL JFC-1600 coater. Micrographs were acquired at 10 kV and magnifications of 50,000× and 100,000×, while preliminary morphology was also examined at 5000× after gold coating.

2.7. Cellulose Nanofluid Preparation

CNP (0.5 wt%) was dispersed in deionized water (DIW), agitated for 6 h, and subsequently ultrasonicated for 1 h to obtain a homogeneous cellulose nanofluid (CNF). To evaluate the effect of reservoir salinity on CNF behaviour, NaCl was added at concentrations ranging from 0.7-2.7 wt%, followed by swirling for 24 h. This salinity range represents the average formation-water salinity reported for the Malay Basin [41] and therefore provides a reservoir-relevant basis for assessing CNF performance. Under these conditions, CNF was selected as a promising alternative to conventional xanthan gum because its nanoscale cellulose structure provides distinctive rheological and thermal stability characteristics relevant to CEOR. Both CNF and xanthan gum exhibit non-Newtonian, shear-thinning behaviour, which is advantageous during injection because viscosity decreases under high shear, reducing flow resistance [42]. CNF can also form a physically interconnected nanoparticle network that contributes to suspension stability and structural integrity, while its relatively high thermal and chemical stability may help preserve functionality under elevated temperature and salinity [43]. Xanthan gum was therefore used as a benchmark to determine whether CNF could provide comparable or improved rheological performance under reservoir-relevant conditions.

2.7.1. Rheological Analysis

Using a Brookfield RST rheometer, the rheology of bleached-treated acacia cellulose and DES-treated CNP were assessed (Figure 2). For high temperature situations, the rheometer is made up of a temperature control that is coupled to a water bath. Every measurement was performed in a temperature range of 25-80 °C and a shear rate of 1-1000 s^{-1}. The trials were carried out in triplicate and the average was given for repeatability.

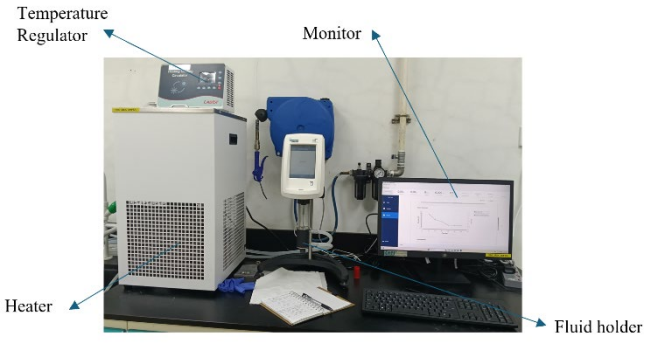

Figure 2. Brookfield DV2T Viscometer for rheology.

2.7.2. IFT measurement

The IFT between crude oil and CNP was measured using a K20 Easy Dyne Kruss tensiometer (Kruss GmbH, Germany) (see Figure 3). The Du-Nouy ring method was used to conduct measurements in air circumstances. This method was used to assess the IFT of CNP dispersions at various concentrations (0.05-0.5 wt%), while examining the effects of temperature (25-80 °C) and NaCl content (0.7-2.7 wt%).

2.7.3. Contact Angle Measurement

Wettability alteration was assessed using the sessile-drop method. Sandstone cores (1 cm thick, 5 cm diameter) were cleaned with DI water and toluene and dried for 24 h. Samples were oil-conditioned in crude oil at 90 °C for 78 h, then exposed to 0.05–0.5 wt% CNP solutions for 78 h and dried. Contact angles were determined using 0.1 cm^3 oil droplets and analyzed with ImageJ.

2.8. Oil Recovery

Sandpack flooding was performed at 25 °C and 14.7 psi using 300 µm quartz sand. The sand was washed, oven-dried at 105 °C for 24 h, and uniformly packed into the holder (Figure 4). Bulk

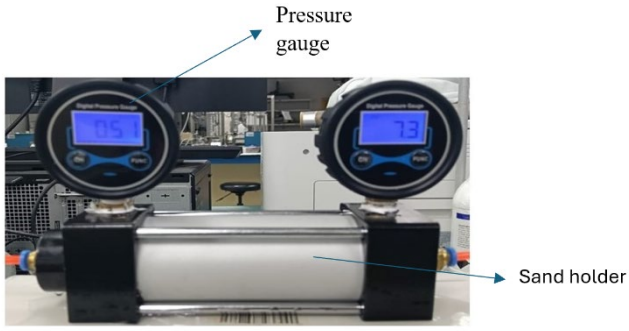

Figure 4. Experimental setup of the sand pack to determine oil displacement.

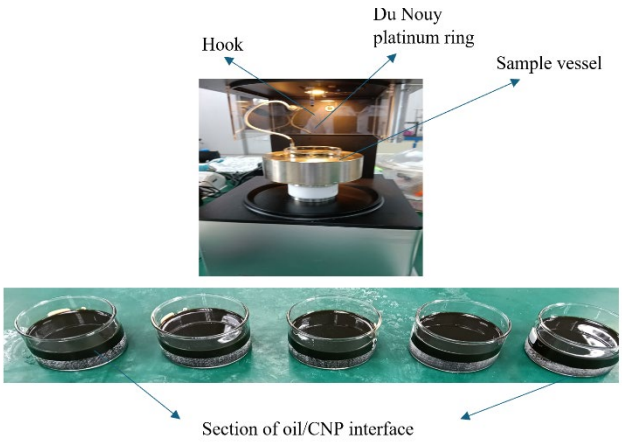

Figure 3. KRUSS K20 Easy Dyne for IFT and Contact Angle.

volume and sand mass were determined from measured dimensions and weighing. The pack was vacuum-saturated with 3.5 wt% NaCl brine to determine pore volume and porosity, while permeability was obtained from steady-state flow using Darcy's law. Crude oil established initial saturation, followed by waterflooding and approximately 1.0 PV CNF injection for tertiary recovery. Cumulative oil production was recorded throughout flooding.

The bulk volume was calculated using Equation (6):

$$(Vb) = \pi \left(\frac{D}{2}\right)^2 \times L \quad (6)$$

whereas D (cm) is the diameter of the consolidated sand in the sandpack holder, L (cm) is the length of the sandpack holder, V_p (cm^3) is the pore volume and V_b (cm^3) is the bulk volume. The pore volume (V_p) was calculated using Eq. (7):

$$V_p = \frac{W_{Sat} - W_{Dry}}{\rho_{brine}} \quad (7)$$

where W_{dry} is the weight of dry sandpack, W_{sat} is the weight of the saturated sandpack filled with brine, the density of brine, ρ_{brine} (1.02 g/mL).
The porosity was calculated using Eq. (8):

$$\phi = \frac{V_p}{V_b} \times 100\% \quad (8)$$

where ϕ is the porosity, V_b is the bulk volume and V_p is the pore volume. The permeability (k) of the sandpack is calculated using Eq. (9):

$$k = \frac{Q\mu L}{A\Delta P} \quad (9)$$

where k is permeability in Darcy, Q is flow rate in mL/min, L (cm) is the length of the sand pack tube, μ is the viscosity of water, A is the cross-sectional area (cm^2) of the tube, and ΔP (atmosphere) is the pressure difference. The OOIP was determined as shown in Eq. (10):

$$OOIP = V_p \times S_{oi} \quad (10)$$

where V_p is the pore pore and S_{oi} is the initial oil saturation. Recovery Factor (RF) from the secondary recovery method was determined using Eq. (11):

$$RF_{wf} = \frac{V_{op}}{OOIP} \times 100\% \quad (11)$$

where V_{op} denotes cumulative oil produced during waterflooding (cm^3), while $OOIP$ represents original oil in place (cm^3). Residual oil was subsequently subjected to CNF–xanthan tertiary flooding. All experiments were conducted in duplicate to ensure reproducibility.

3. Results and Discussions

3.1. Yield (%) Cellulose and Cellulose Nanoparticles (CNP)

Sequential alkaline and bleaching pretreatment effectively removed lignin, hemicellulose, and other impurities from Acacia auriculiformis bark. Treatment with 5% (w/v) NaOH followed by 3 wt% NaClO yielded 72.9% cellulose (Table 3), indicating effective delignification and purification. This value is comparable with reported cellulose yields of 84.85% from OPEFB [44] and 57.5% from coffee pulp [45]. DES-assisted hydrolysis subsequently produced CNPs, with the optimum condition of ChCl = 1:1, 100 °C, 4 h, and 20 wt% water achieving an average yield of 78.3%. Water addition reduced DES viscosity, enhanced solvent penetration and fibre swelling, and facilitated lignin and hemicellulose removal. Conversely, anhydrous DES limited mass transfer because of its higher viscosity. The obtained yield agrees with reported DES-based cellulose yields of 78-84% for OPEFB, 65.2% for MCC, and 60.2% for wheat-straw CNCs [19,22], confirming the effectiveness of the proposed extraction route [46,47].

Table 3. Previous research studies on Cellulose and CNP yield (%).

Biomass waste	DES	Conditions	Yield (%)	References
Acacia bark	ChCl/CA (1:1)	Temp.: 100 °C; Time: 4 h	Cellulose: 72.9%; CNP: 78.3%	This study
OPEFB	ChCl/OA (1:1)	Time: 90 °C; Time: 15 min	Cellulose: 84.85%; CNP: 87%	[44]
Sterculia Foetida shell (SFS)	ChCl/LA (1:2)	Time: 110 °C; time: 120 min	Cellulose: 30.6±0.84%; CNP: 88.07%	[48]
Oil Palm Trunk (OPT)	ChCl/Levulinic acid	Time: 104.2 °C; time: 3.76 h	Cellulose: 91.29%	[49]
Hemp fibres	ChCA/LA	Time: 2-4h	Cellulose: 78-91%	[50]

3.2. Characterization of Cellulose and CNPs

Figure 5(a) shows the FTIR spectra of bleached Acacia auriculiformis cellulose (ACA-bleached) and DES-derived cellulose nanoparticles (ACA-CNP). Both samples exhibited characteristic cellulose I bands at 3350 cm^{-1} (O–H), 2900 cm^{-1} (C–H), 1640 cm^{-1} (adsorbed H_2O), 1410 cm^{-1} (CH_2), 1330 cm^{-1} (C–H), 1170 cm^{-1} (C–O–C), 1050 cm^{-1} (C–O), and 897 cm^{-1} (β-(1,4)-glycosidic linkage) [51]. The broader, stronger 3350 cm^{-1} band in ACA-CNP indicates increased hydroxyl accessibility following lignin and hemicellulose removal, whereas disappearance of the 2900 cm^{-1} band suggests elimination of residual aliphatic constituents [52]. Preservation of the 1640, 1050, and 897 cm^{-1} bands confirm retained cellulose structure. DES selectively disrupts lignin–carbohydrate interactions, while ultrasonication releases nanoscale crystallites without cleaving β-(1,4)-glycosidic bonds [53,54]. These structural changes enhance surface functionality and interfacial reactivity, supporting EOR applications [55,56].

Figure 5(b) presents the XRD patterns of bleached Acacia auriculiformis cellulose and ACA-CNP. Both samples exhibited characteristic cellulose I reflections at 2θ = 15°, 16.5°, 22.7°, and 34.7°, corresponding to the (1-10), (110), (200), and (004) planes, respectively [57]. The retained diffraction profile confirms preservation of the native cellulose I structure following DES

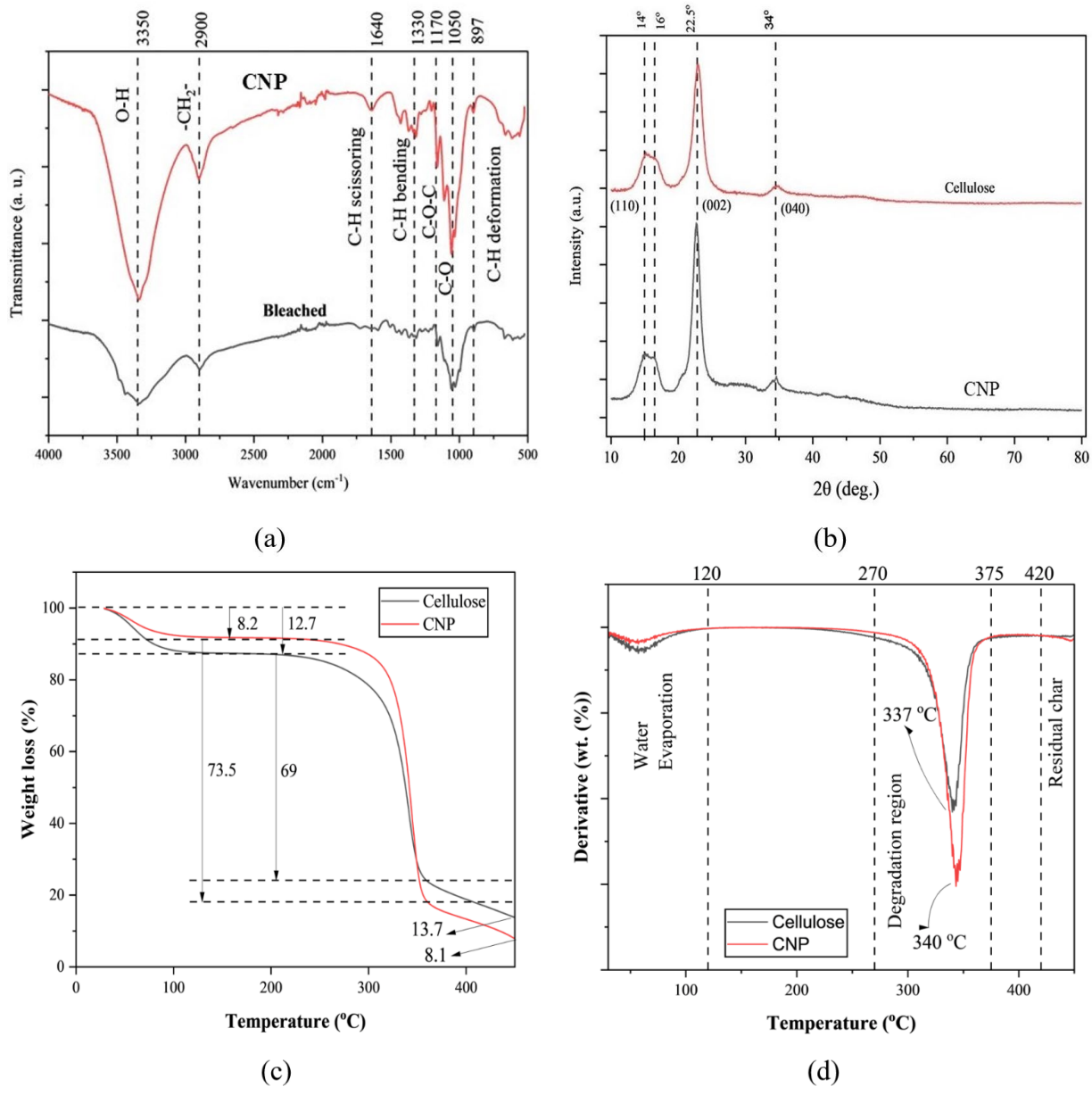

Figure 5. Characterization of bleached Acacia auriculiformis cellulose and CNPs: (a) FTIR spectra, (b) XRD patterns, (c) TGA profiles showing mass loss, and (d) DTA thermograms of bleached cellulose and DES-treated CNPs.

treatment and ultrasonication. The dominant (200) reflection at 22.7° remained evident, although its lower intensity in ACA-CNP suggests partial crystalline-domain disruption during processing [58]. Nevertheless, selective removal of amorphous lignin, hemicellulose, and disordered cellulose increased the relative crystalline fraction. Accordingly, CrI increased slightly from 75.9% for bleached cellulose to 76.6% for ACA-CNP, demonstrating effective fractionation with minimal structural damage as shown in Table 4 [59,60]. These values compare with reported CrI values of 84% for mustard-straw CNPs and 68% for carpentry-wood CNPs [61], confirming the suitability of DES-assisted hydrolysis for producing structurally stable Acacia CNPs.

Figure 5(c) presents the TGA, DTG, and DTA profiles of bleached Acacia auriculiformis cellulose and CNPs, revealing similar overall thermal degradation behaviour. The initial mass loss below 120 °C is attributed to evaporation of physically adsorbed moisture, while the principal degradation region corresponds to dehydration, depolymerization, and cleavage of cellulose glycosidic linkages [69,70]. At 650 °C, residual masses of 13.7% and 8.1 wt% were recorded for bleached cellulose and CNPs, respectively. The greater residue of bleached cellulose may reflect residual inorganic constituents or pretreatment-derived residues. DTG analysis (Figure 5(d)) showed a maximum degradation temperature (T_{max}) of approximately 337 °C for bleached cellulose, whereas CNPs exhibited an additional peak near 150 °C, potentially associated with thermally labile citrate-derived surface groups. Overall, degradation occurred in three stages: moisture and amorphous-component removal (25-120 °C), cellulose decomposition (250-300 °C), and carbonization (400-650 °C). DTA profiles showed endothermic events below 120 °C and at 330-360 °C, corresponding to moisture evaporation and cellulose degradation, respectively [70]. The sharper CNP endotherm indicates greater structural uniformity and crystalline enrichment following DES treatment, confirming effective purification and nanocrystal formation [71].

3.3. SEM & FESEM

Figure 6 presents the SEM micrographs of bleached Acacia auriculiformis cellulose (ACA-bleached) and DES-derived cellulose nanoparticles (ACA-CNP). The colour change from brown to pale yellow after alkaline and bleaching treatment indicates progressive removal of lignin, hemicellulose, and extractives. Morphologically, ACA-bleached exhibited rough, partially separated fibrils, whereas ACA-CNP showed well-dispersed, rod-like nanoparticles with an average diameter of 19.65±0.2 nm (Figure 7), confirming successful nanocrystal isolation [72]. The absence of pronounced agglomeration further indicates effective DES-assisted fibrillation and favourable dispersion.

The morphological transformation can be attributed to the synergistic effects of pretreatment and DES hydrolysis. Alkaline

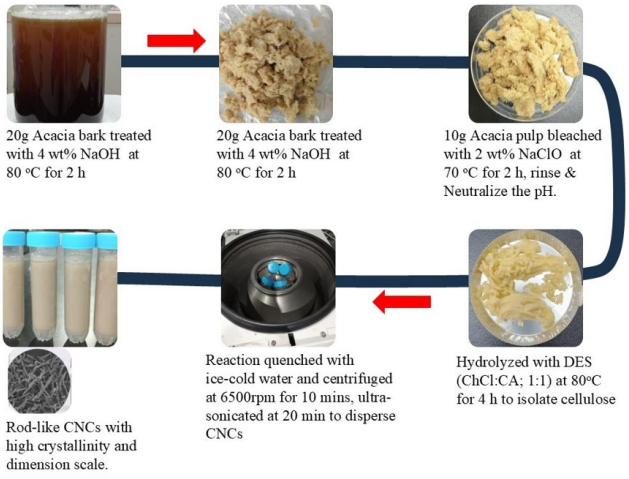

Figure 6. Acacia auriculiformis bark delignification and hydrolysis via DES.

Table 4. Crystallinity Index (CI).

Biomass waste	DES ratio	Conditions	Crystallinity Index (CI%)	References
Acacia bark	ChCl/CA (1:1)	Temp: 100 °C; time: 4 h	76.6%	This study
SCB	ChCl/Urea (1:2)	Temp: 130 °C; time: 2 h	56.7-57.2	[62]
Hemp fibres	ChCl/LA	Time: 2-4 h	89.9%	[63]
Sargassum spp. Biomass	ChCl/OA (1:1)	-	86%	[64]
Kenaf fiber	ChCl/LA (1:2)	-	81.2	[65]
Untreated Sorghum bicolor stalk (SBS)	ChCl/Urea (1:2)	-	45.05 ±0.1%	[66]
Acid hydrolyzed poplar chips	ChCl/LA	-	80	[67]
Cotton wool	ChCl.Gallic acid	-	80	[68]

treatment promotes fibre swelling and hemicellulose removal, while bleaching oxidizes and solubilizes residual lignin. Subsequently, DES preferentially removes amorphous regions while preserving the ordered crystalline domains [73]. Ultrasonication further disrupts interfibrillar interactions, facilitating nanocrystal separation while maintaining structural integrity [74]. The resulting nanoscale structure provides high surface area and accessible hydroxyl groups, which can enhance interfacial interactions and support nanocomposite and EOR applications [75,76].

3.4. Rheological Behaviour of CNP and Xanthan under Varying Salinity and Temperature Conditions

Figure 8(a) shows that Acacia CNP exhibited shear-dependent non-Newtonian behaviour comparable to xanthan gum, but with higher apparent viscosity at 2.2 wt%, indicating stronger particle-particle and particle-fluid interactions. The CNP suspension displayed three-region behaviour: shear thinning at low shear, an intermediate viscosity plateau, and further thinning at high shear due to progressive alignment and reorganization of rod-like nanoparticles [77,78]. Enhanced viscosity may also arise from electroviscous effects, whereby surface charges and electrical double layers increase effective hydrodynamic volume and flow resistance [79,80]. These characteristics demonstrate the potential of Acacia CNP for effective mobility control during EOR.

Figure 8(b) shows that increasing NaCl concentration progressively reduced the apparent viscosity of both Acacia CNP and xanthan gum at 2.2 wt%, while preserving shear-thinning

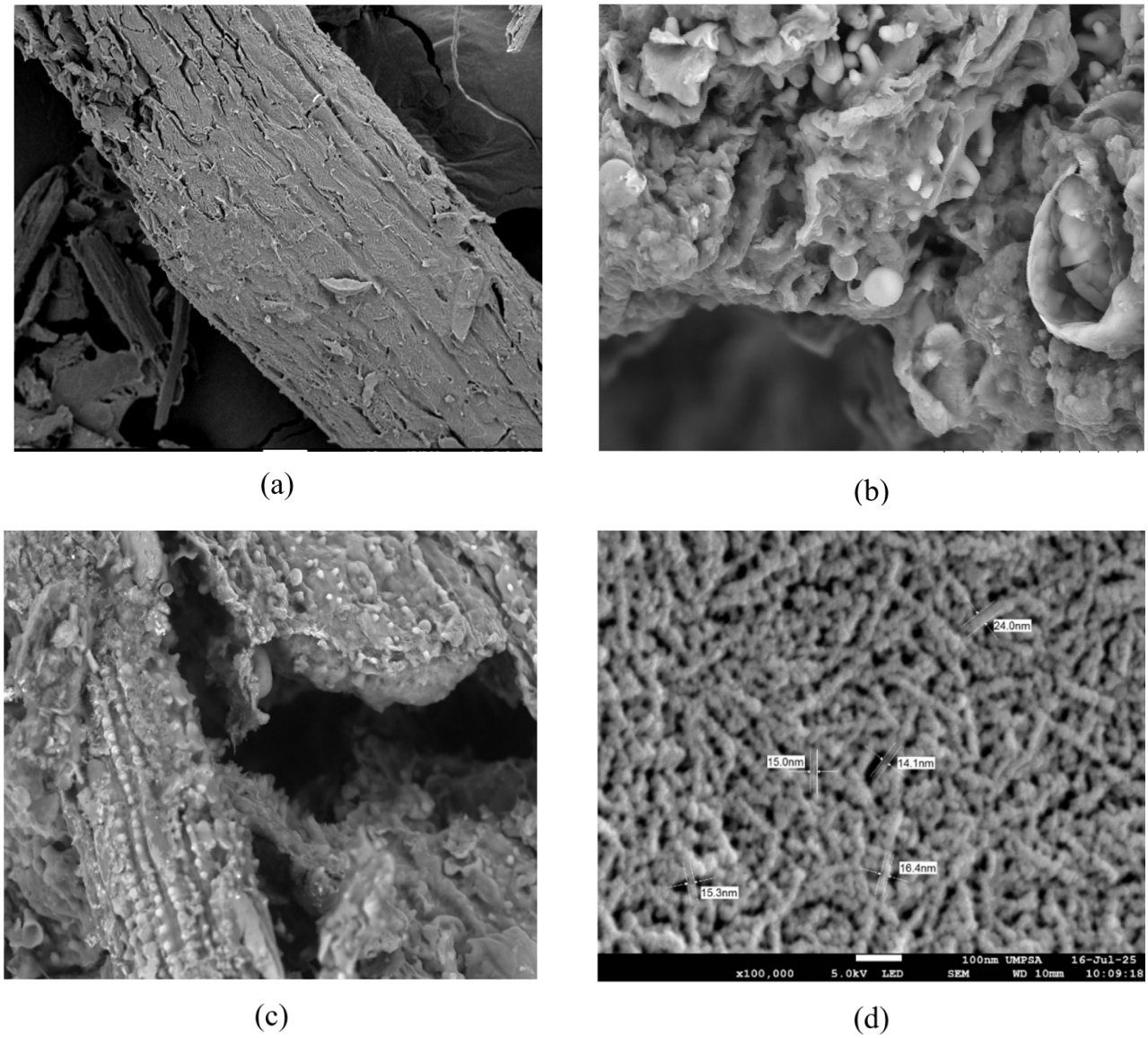

Figure 7. SEM micrograph images at (a) alkali treated acacia bark (b) bleached acacia pulp (c) DES treated acacia (d) FESEM images of acacia bark.

behaviour. The stronger viscosity decline observed for CNP indicates greater ionic-strength sensitivity. This reduction is primarily attributed to Na^+-induced compression of the electrical double layer, which weakens interparticle repulsion and reduces effective hydrodynamic volume and electroviscous effects [81,82]. Nevertheless, persistent shear thinning indicates that salinity altered viscosity magnitude rather than the fundamental flow mechanism, as CNPs progressively align under shear [83]. At excessive ionic strength, further charge screening may induce aggregation [4,84]. Acacia CNP maintained favourable rheological behaviour under saline conditions, supporting its potential for mobility control in high-salinity EOR [85], [86].

Figure 8(c) compares the temperature-dependent rheology of Acacia CNP and xanthan at 2.2 wt% over 25-80 °C. Xanthan viscosity decreased progressively with temperature because increased molecular mobility weakened intermolecular associations and reduced polymer-chain resistance to flow. In contrast, Acacia CNP viscosity increased, suggesting temperature-induced changes in hydration, Brownian motion, and particle-particle interactions rather than changes in surface area [87]. Temperature may promote reorganization of rod-like CNPs and strengthen transient structures, thereby increasing flow resistance [88,89]. The observed viscosity enhancement indicates potential for high-temperature EOR mobility control. However, thermal-aging studies are required to distinguish reversible structural changes from aggregation or degradation [90].

3.5. Effect of CNF and Xanthan Concentration on IFT

Figure 9(a) shows a concentration-dependent reduction in oil–water IFT following CNF addition. The initial IFT values were 24.4 mN/m for CNF and 26.7 mN/m for xanthan, decreasing to 18.2 mN/m and 19.53 mN/m, respectively. Thus, CNF exhibited greater interfacial activity, achieving approximately 19.9% IFT reduction. This behaviour is attributed to CNF adsorption and accumulation at the oil–water interface, forming a denser interfacial layer that lowers interfacial free energy [91]. The superior performance of CNF may result from its high aspect ratio, specific surface area, and adsorption capacity, whereas excessive xanthan may promote aggregation. Reduced IFT can decrease capillary trapping and facilitate residual-oil mobilization, highlighting CNF's potential as a bio-based EOR additive [92,93].

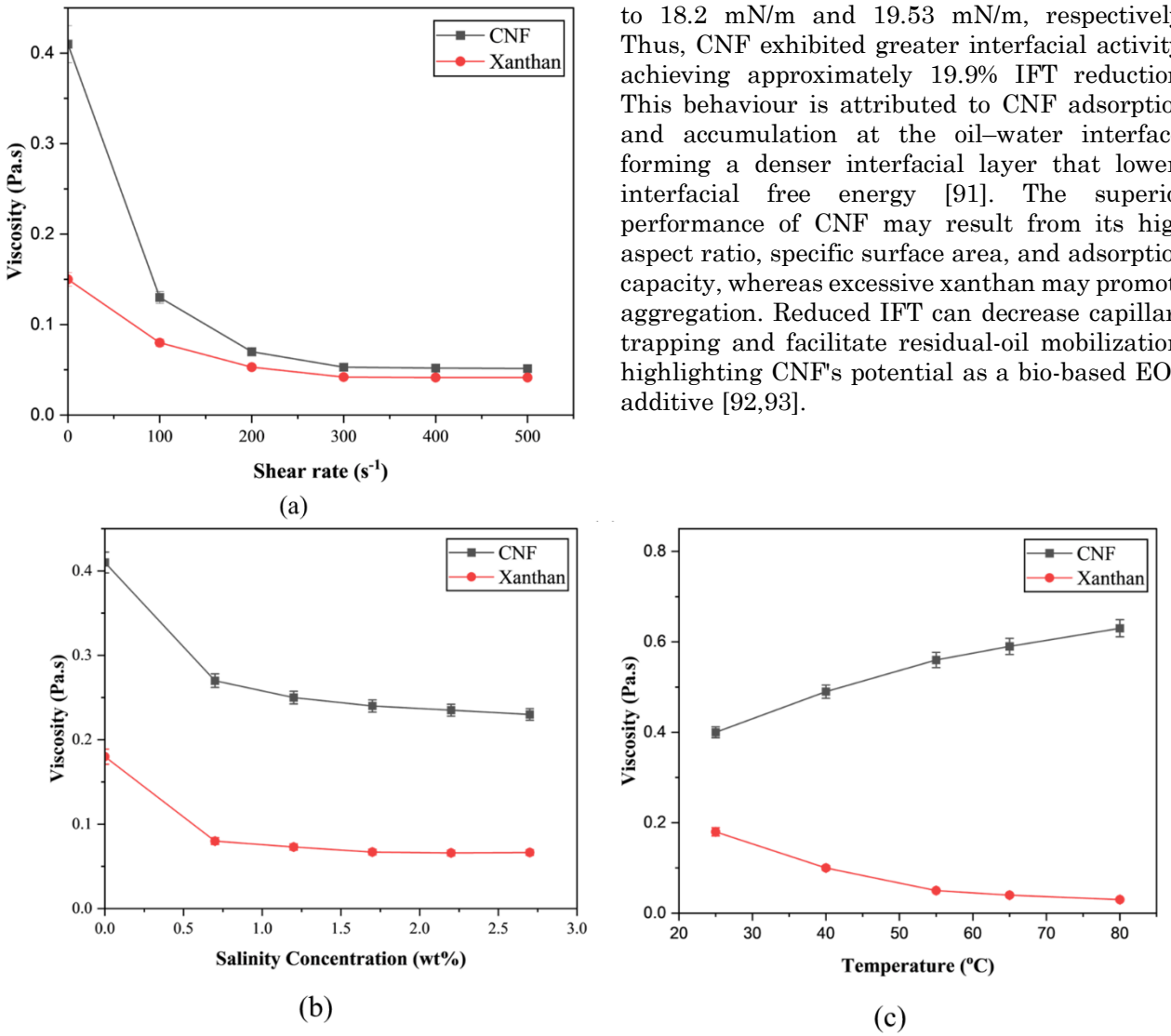

Figure 8. Rheological characteristics of CNF and xanthan: (a) shear-rate-dependent behaviour, (b) effect of salinity on apparent viscosity, and (c) temperature dependence of apparent viscosity.

Figure 9(b) shows a non-monotonic effect of NaCl concentration on oil–water IFT. Increasing salinity from 0.7 to 2.2 wt% reduced CNF IFT from 17.5 to 12.3 mN/m (29.7%), compared with 19.6 to 15.8 mN/m (19.4%) for xanthan. The reduction is attributed to ionic-strength-induced electrical double-layer compression, enhanced CNF adsorption, and improved interfacial packing [94,95]. The minimum IFT occurred at 2.7 wt% NaCl, suggesting an optimum balance among CNF dispersion, hydration, and interfacial adsorption. At excessive salinity, further charge screening may promote aggregation and reduce interfacial availability [96]. The resulting IFT reduction can lower capillary resistance and facilitate residual-oil mobilization, although wettability and capillary forces must also be considered [97].

Figure 9(c) shows a monotonic decrease in oil–CNF IFT as temperature increased from 25 to 80 °C. At 80 °C, CNF and xanthan achieved IFT reductions of 51.9% and 48.6%, corresponding to decreases of 7.6 and 9.4 mN/m, respectively. The greater percentage reduction for CNF indicates stronger interfacial activity at elevated temperatures. Increased molecular mobility enhances CNF transport, adsorption, and interfacial rearrangement, producing a more stable interfacial layer and lowering interfacial free energy [98,99]. Unlike some inorganic nanoparticles, CNF showed no apparent temperature-induced aggregation, retaining IFT-reducing capability up to 80 °C. This thermal stability can reduce capillary resistance and facilitate residual-oil mobilization during EOR [100,101].

3.6. The Effect of CNF and Xanthan Concentration on Contact Angle

Figure 10(a) shows a concentration-dependent shift from oil-wet toward water-wet conditions after CNF and xanthan treatment. The initial contact angle was 128°; at 0.05 wt%, it decreased to 110.2° for xanthan and 84.3° for CNF. At 0.5 wt%, the angles further declined to 75.2° and 58.8°, respectively, confirming superior wettability alteration by CNF. The reduction is attributed to structural disjoining pressure generated as CNF accumulates near the oil–rock–water contact line, forming a wedge-shaped film that separates oil from the rock surface [102]. Increasing CNF concentration strengthens this film through enhanced particle interactions and electrical-double-layer effects. The greater CNF response reflects its favourable size, surface

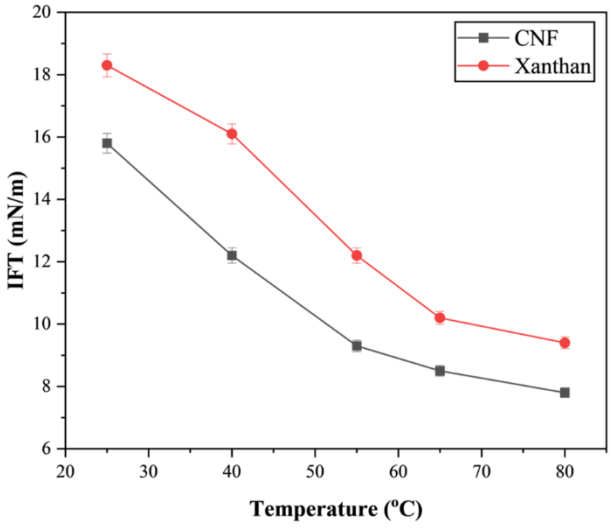

(c)

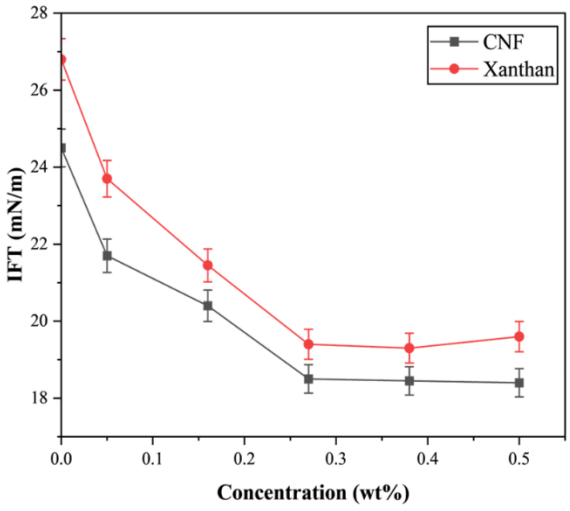

(a)

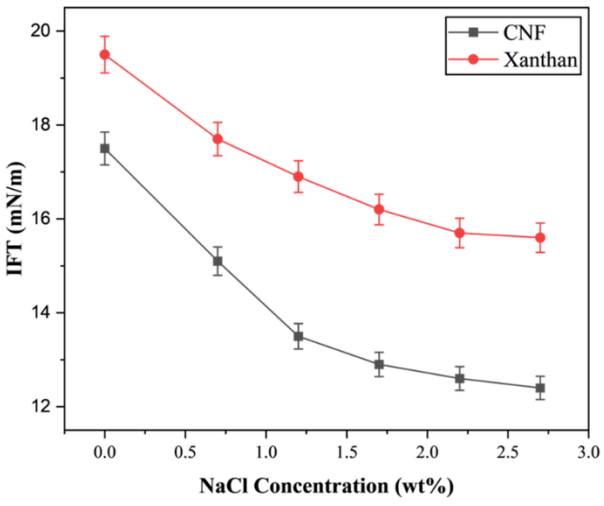

(b)

Figure 9. Effects of (a) CNF and xanthan concentration on IFT, (b) NaCl concentration on IFT reduction, and (c) temperature on the IFT of CNF and xanthan systems.

charge, dispersion, and interfacial mobility. Consequently, CNF-induced water-wetness reduces oil adhesion and promotes residual-oil mobilization [103].

Figure 10(b) shows that NaCl concentration influenced the wettability alteration of both xanthan and CNF. At low salinity, both agents shifted sandstone from oil-wet toward water-wet conditions; however, increasing salinity progressively weakened xanthan performance, producing intermediate wettability. In contrast, CNF maintained water-wet conditions, achieving a contact angle of 36.2° compared with 50.1° for xanthan, demonstrating superior salt tolerance. At low ionic strength, enhanced electrical-double-layer (EDL) interactions increase electrostatic repulsion and disjoining pressure, promoting oil detachment [104,105]. Higher salinity compresses the EDL, reducing repulsion and promoting particle aggregation and sedimentation [106]. Nevertheless, CNF maintained an optimum contact angle of 36.2° at 2.2 wt% NaCl, indicating greater dispersion stability and interfacial robustness under saline conditions [107,108].

Figure 10(c) shows a pronounced temperature-dependent wettability alteration for CNF and xanthan. Increasing temperature from 25 to 80 °C reduced contact angles from 130.5° to 16.5° for CNF and 135.1° to 48.9° for xanthan, corresponding to reductions of 87.3% and 63.8%, respectively. The stronger CNF response reflects enhanced molecular mobility, reduced oil viscosity and interfacial energy, and improved nanoparticle transport toward the oil–water–rock interface [109,110]. CNF may also form a thin aqueous film that reduces oil–rock adhesion, while structural disjoining pressure promotes oil detachment [111]. The pronounced change between 30-60 °C likely results from these combined effects. Continuous wettability improvement to 80 °C further indicates favourable thermal stability of CNF under the tested conditions [112].

3.7. Oil Displacement Experiments

Figure 11 demonstrates the superior EOR performance of CNF relative to xanthan during core flooding. Water flooding recovered 53.3% OOIP, leaving considerable residual oil. Subsequent CNF flooding increased recovery to 75.7% RF, compared with 63.1% RF for xanthan, corresponding to additional recoveries of 22.4% OOIP and 9.8% OOIP, respectively [113,114]. The enhanced CNF performance reflects a synergistic combination of mobility control, wettability alteration, IFT reduction, and interfacial

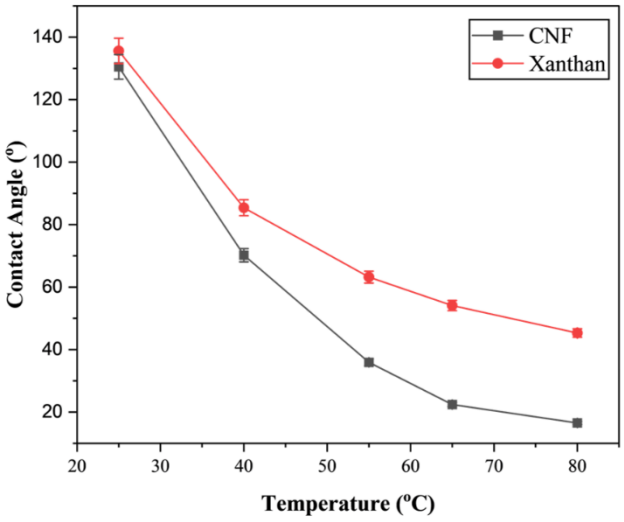

(c)

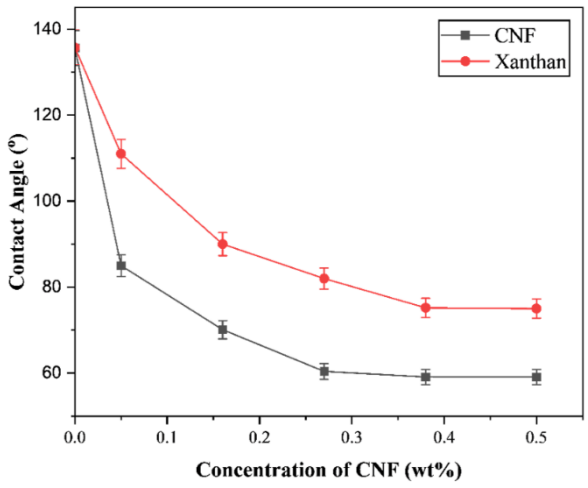

(a)

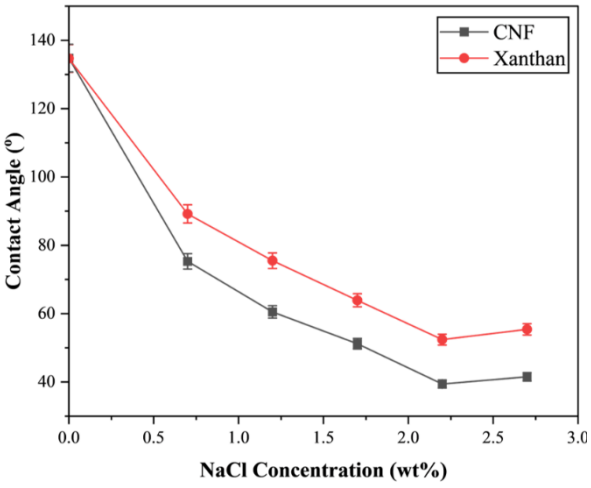

(b)

Figure 10. Wettability characteristics of CNF and xanthan: (a) effect of concentration on contact angle, (b) influence of NaCl concentration on contact angle, and (c) temperature-dependent contact-angle variation.

disjoining pressure rather than viscosity enhancement alone [115].

At the macroscopic scale, the higher CNF viscosity improves the mobility ratio and promotes more efficient sweep of previously unswept regions. Microscopically, its lower IFT and stronger shift toward water-wetness reduce oil–rock adhesion and facilitate residual-oil deformation and detachment. Moreover, CNF accumulation near the three-phase contact region can generate structural disjoining pressure and form a wedge-shaped aqueous/nanoparticle film, further promoting oil displacement [116]. Thus, the markedly higher recovery achieved by CNF indicates that interfacial mechanisms, particularly wettability alteration, complemented by improved rheology, govern its superior EOR performance.

4. Conclusion

This study successfully developed an environmentally compatible CNF from Acacia auriculiformis biomass and demonstrated its potential for sustainable EOR. Process intensification influenced CNP formation and properties, with SEM/FESEM confirming predominantly cylindrical particles of 19.65 ± 0.2 nm. FTIR verified characteristic cellulose functional groups, while XRD confirmed structural integrity and a crystallinity index (CrI) of 76.6%. Rheological analysis showed shear-thinning and pseudoplastic behaviour for both CNF and xanthan; however, CNF exhibited superior viscosity retention under saline conditions, supporting its mobility-control potential in harsh reservoirs. CNF also demonstrated stronger interfacial and wettability performance. At elevated temperature, CNF reduced IFT to 7.4 mN/m, compared with 9.2 mN/m for xanthan, while contact angles decreased to 16.5° and 49.3°, respectively, indicating a stronger transition toward water-wetness. These effects are attributed to enhanced CNF adsorption, molecular mobility, and favourable oil-brine-rock interactions, which reduce oil-rock adhesion and promote residual-oil mobilization. Most importantly, core flooding yielded 22.4% incremental oil recovery with CNF versus 9.8% for xanthan. Collectively, these results establish Acacia-derived CNF as a promising and sustainable alternative to conventional chemical EOR agents. However, further work is required to translate this laboratory performance into field applicability through pilot- and field-scale validation of CNF injectivity, transport, pressure response, thermal-salinity stability, wettability alteration, and recovery efficiency under representative HTHS reservoir conditions. In parallel, long-term durability and process optimization should address DES composition, recycling, feedstock pretreatment, surface functionalization, CNF retention, and injectivity, supported by long-term HTHP flooding, techno-economic analysis, and life-cycle assessment to establish the technical, economic, and environmental feasibility of large-scale deployment.

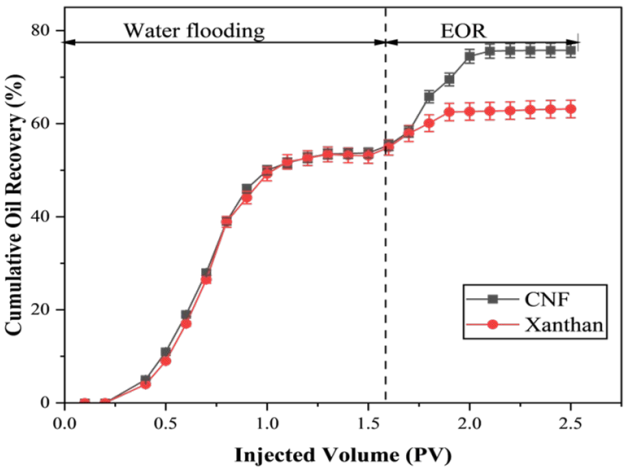

Figure 11. Comparative oil recovery performance of CNF and xanthan.

Acknowledgment

The work was financially supported by the Ministry of Higher Education (MOHE) Malaysia and Universiti Malaysia Pahang Al-Sultan Abdullah through research grant RDU 230304.

CRedit Authors Statement

Author Contributions: Francis Nyah contributed to the conceptualization, methodology, formal analysis, investigation witing draft and visualization. Abutu David participated in formal analysis. Kufre Mkpadem participated in usage of software and project administration. Money Barima participated in investigation. Okorie Agwu participated in validation and visualization. Norida Ridzuan contributed to the conceptualization, validation, resources, supervision and funding acquisition. All authors have read and agreed to the published version of the manuscript.

References

[1] Zadmehr, M., Perrons, R.K., Desouza, K.C. (2026). The impact of geopolitical risks on the dynamic capabilities of Big Oil. *Energy Res. Soc. Sci.*, 134, 104612. DOI: 10.1016/j.erss.2026.104612.

[2] Abutu, D., Yussof, H.W., Nyah, F., Nwaichi, P.I., Umunnawuike, C., Agi, A. (2026). Modelling biohydrogen production from residual hydrocarbons by immobilized bacteria using COMSOL Multiphysics. *Biomass Bioenergy*, 211, 109165. DOI: 10.1016/j.biombioe.2026.109165.

[3] Rezvani, H., Binks, B.P., Nguyen, D. (2024). Surfactant-Nanoparticle Formulations for Enhanced Oil Recovery in Calcite-Rich Rocks. *Langmuir*, 40(47), 24989–25002. DOI: 10.1021/acs.langmuir.4c03100.

[4] Musa, M.S.M., Damin, R., Yekeen, N., Nwaichi, P.I., Umunnawuike, C., Nyah, F., Abutu, D., Money, B., Gbonhinbor, J., Nwaichi, E.O., Agi, A. (2025). Experimental Assessment of the Rheological Behaviours and Enhanced Oil Recovery Potentials of Pectin. *SPE Nigeria Annual International Conference and Exhibition*, SPE. Aug. 2025. DOI: 10.2118/228639-MS.

[5] Chen, X., Li, Y.-Q., Liu, Z.-Y., Trivedi, J., Gao, W.-B., Sui, M.-Y. (2023). Experimental investigation on the enhanced oil recovery efficiency of polymeric surfactant: Matching relationship with core and emulsification ability. *Pet. Sci.*, 20(1), 619–635. DOI: 10.1016/j.petsci.2022.11.002.

[6] Sun, X., Bai, B., Alhuraishawy, A.K., Zhu, D. (2021). Understanding the Plugging Performance of HPAM-Cr (III) Polymer Gel for CO2 Conformance Control. *SPE Journal*, 26(5), 3109–3118. DOI: 10.2118/204229-PA.

[7] Marquez, R., Ding, H., Barrios, N., Vera, R. E., Salager, J-L., Al-Shalabi, E.W., Mettu, S. (2025). Recent Advances in Enhanced Oil Recovery with Low-Salinity Waterflooding and Its Hybrid Methods in Carbonate Reservoirs. *Energy & Fuels*, 39(19), 8769–8799. DOI: 10.1021/acs.energyfuels.4c06023.

[8] Hassan, A.M., Al-Shalabi, E.W., Ayoub, M.A. (2022). Updated Perceptions on Polymer-Based Enhanced Oil Recovery toward High-Temperature High-Salinity Tolerance for Successful Field Applications in Carbonate Reservoirs. *Polymers (Basel).*, 14(10), 2001. DOI: 10.3390/polym14102001.

[9] Zhang, G., Ran, Y., Jiang, P., Pei, H. (2023). A Study on the Thermal Degradation of an Acrylamide and 2-Acrylamido-2-Methylpropanesulfonic Acid Copolymer at High Temperatures. *Polymers (Basel).*, 15(12), 2665. DOI: 10.3390/polym15122665.

[10] Jing, Z., Liu, C., Qi, R., Ren, P. (2018). Many-body effect determines the selectivity for Ca $^{2+}$ and Mg $^{2+}$ in proteins. *Proceedings of the National Academy of Sciences*, 115(32), Aug. 2018. DOI: 10.1073/pnas.1805049115.

[11] Nyah, F., Ridzuan, N., Epelle, E., Aziz, M.A.B., Money, B., Abutu, D., Agi, A. (2025). Cellulose bionanomaterial design for enhanced oil recovery: A review of existing, emerging technologies and future outlook. *Petroleum Research*. 101(2), 641-686. DOI: 10.1016/j.ptlrs.2025.12.002.

[12] Ikeagwu, C., Nyah, F.J., Onyekonwu, M.O., Ogolo, N.A., Ubani, C. (2013). Study of Alcohol Mixtures for Enhanced Oil Recovery. *SPE Nigeria Annual International Conference and Exhibition*, SPE, Aug. 2013. DOI: 10.2118/167547-MS.

[13] Umunnawuike, C., Abutu, D., Nwaichi, P.I., Nyah, F., Agi, A. (2026). Thermophilic biohydrogen production from reservoir residual hydrocarbons using palm oil mill effluent–derived microbial consortia. *Science of The Total Environment*, 1016, 181482, Feb. 2026. DOI: 10.1016/j.scitotenv.2026.181482.

[14] Khormali, A., Ahmadi, S. (2026). Optimization of HPAM Polymer Flooding for Enhanced Oil Recovery Through Experimental Core Flooding and Predictive Statistical Modeling, *Polymers (Basel)*, 18(13), 1640. DOI: 10.3390/polym18131640.

[15] Cancela, B.R., Palermo, L.C.M., de Oliveira, P.F., Mansur, C.R.E. (2022). Rheological study of polymeric fluids based on HPAM and fillers for application in EOR. *Fuel*, 330, 125647, Dec. 2022, DOI: 10.1016/j.fuel.2022.125647.

[16] Sarokolai, F.T., Shiri, Y. (2025). Titanium dioxide-grafted polyacrylamide nanocomposites ameliorate the rheology and high-pressure high-temperature fluid loss of water-based drilling fluids. *Results in Engineering*, 27, 106624. DOI: 10.1016/j.rineng.2025.106624.

[17] Ali, I., Han, S., Tian, L., Huang, C., Zhazitov, M., Duisebayev, T., Sagidolda, Y., Ali, M.Z., Toktarbaiuly, O., Xu, Y., Liu, J. (2026). Advancements in polymeric superhydrophobic nanocomposite coatings: From synthesis to industrial applications. *Review of Materials Research*, 2(5), p100202, May 2026, DOI: 10.1016/j.revmat.2026.100202.

[18] Mondal, M.C., Uddin, H.M.W., Progoti, Q.R.M., Tushar, M.A-N., Dutta, A., Saif, T., Malitha, S.B. (2026). Enhanced oil recovery via metal oxide nanoparticles: A review of recent advancements, core mechanisms, and future outlook. *Next Materials*, 12, 102004. DOI: 10.1016/j.nxmate.2026.102004.

[19] Wang, C., Jin, G., Wang, W., Zhao, C., Wang, S., Zhao, Y., Ni, J. (2026). Nanomaterials Driving Technological Advancements in Enhanced Oil Recovery from Low-Permeability Tight Oil Reservoirs: Opportunities and Challenges. *Nanomaterials*, 16(8), 464. DOI: 10.3390/nano16080464.

[20] Peng, Y., Han, F., Zhao, Y., Wang, H., Gong, J., Wu, K. (2025). Research on wettability and interaction mechanism of silica nanoparticles on coal surface: Based on experiments and molecular dynamics simulations. *Appl. Surf. Sci.*, 713, 164266, Dec. 2025, DOI: 10.1016/j.apsusc.2025.164266.

[21] Matarneh, S., El-Rayyes, A., Bahl, A., Sathish, T., Kavisri, M., Moovendhan, M. (2026). Silica nanoparticle-induced modulation of oil–water interfacial dynamics for enhanced oil recovery. *Surfaces and Interfaces*, 96, 109829, Sep. 2026. DOI: 10.1016/j.surfin.2026.109829.

[22] Vaganov, R.A., Zhigarev, V.A., Pryazhnikov, M.I., Shebeleva, A.A., Nemtsev, I.V., Minakov, A.V. (2026). Improving the efficiency of surfactant and polymer solutions by modifying them with nanoparticle additives to increase oil recovery. *Chem. Eng. Sci.*, 321, 122732. DOI: 10.1016/j.ces.2025.122732.

[23] Xu, X., Meng, C., Zhan, J., Wang, Q., Zhang, M., Wang, C., Pan, J., Cui, H., Zhao, X. (2026). Nanoparticle-plant interactions: Uptake, transport, physiological effects, and environmental implications. *Journal of Hazardous Materials Advances*, 22, 101123. DOI: 10.1016/j.hazadv.2026.101123.

[24] Bendaoued, A., Messaoud, M., Harzallah, O., Bistac, S., Salhi, R. (2022). Nano-TiO2 effect on thermal, rheological and structural properties of thermoplastic polypropylene nanocomposites. *Journal of Materials Research and Technology*, 17, 2313–2325, Mar. 2022, DOI: 10.1016/j.jmrt.2022.01.114.

[25] Haruna, M.A., Tangparitkul, S., Wen, D. (2024). Dispersion of polyacrylamide and graphene oxide nano-sheets for enhanced oil recovery. *Colloids Surf. A Physicochem. Eng. Asp.*, 699, 134689, DOI: 10.1016/j.colsurfa.2024.134689.

[26] Djouonkep, L.D.W., Xie, B., Tao, H., Chen, J., Zhuo, L., Selabi, N.B.S., Zhao, L. (2024). Enhanced amphoteric polymer filtration reducer with vinyl-functionalized nanosilica for high-salt and ultra-high temperature water-based drilling environments. *Geoenergy Science and Engineering*, 236, 212743. DOI: 10.1016/j.geoen.2024.212743.

[27] Khedulkar, A.P., Bobade, R.G., Doong, R., Pandit, B., Ky, N.M., Ambare, R., Hoang, TD., Kumar, K.J. (2025). Bio-based nanomaterials as effective, friendly solutions and their applications for protecting water, soil, and air. *Mater. Today Chem.*, 46, 102688. DOI: 10.1016/j.mtchem.2025.102688.

[28] Nyah, F., Ridzuan, N., Aziz. M.A.B.A., Gbonhinbor, J.R., Money, B., Nwaichi, P.I., Umunnawuike, C., Abutu, D., Agi, A. (2025). Bibliometric Insights into Cellulose Nanoparticles: Advancing Sustainable Enhanced Oil Recovery in HTHP Reservoirs. *SPE Nigeria Annual International Conference and Exhibition*, SPE, Aug. 2025. DOI: 10.2118/228643-MS.

[29] Suliman, Z.A., Ibrahim, A.A., Mecha, C.A., Chollom, M.N. (2025). Photocatalytic degradation and antibacterial efficacy of novel synthesized green Cu–Fe metal organic framework derived from Acacia nilotica extract. *Discover Chemistry*, 2(1), 219. DOI: 10.1007/s44371-025-00297-7.

[30] Nguyen, T.T.H., Nyugen, X.C., Nguyen, D.L.T., Nguyen, D.D., Vo, T.Y.B., Vo, Q.N., Nguyen, T.D., Ly, Q.V., Ngo, H.H., Vo, D.-V.H., Nguyen, T.P., Kim, I.T., Le, Q.V., (2023). Converting biomass of agrowastes and invasive plant into alternative materials for water remediation. *Biomass Convers. Biorefin.*, 13(6), 5391–5406. DOI: 10.1007/s13399-021-01526-6.

[31] Mary, P.P., Kumaresavanji, M., Venkatesh, P.S., Kannan, N., Ragupathy, P., Vasumathi, V. (2026). Upcycling Acacia auriculiformis leaf waste into Eco- Graphite: A sustainable route to high-performance rGO-MoO3 photocatalysts. *Emergent Mater.*, 9(1–3), 34. DOI: 10.1007/s42247-026-01362-2.

[32] Chavda, V., Borah, P., Thakur, M., Patil, Y., Bhargawa, B., Gandhi, M., Lee, Y-S., Ghotekar, S., Jain, P., Raghav, S., Yadav, A. K., Kim, W., Ahmaruzzaman, Md., (2026). Deep eutectic solvent engineered metal–organic frameworks (DES-MOFs): A green pathway toward next-gen advanced functional materials. *Chemical Engineering Journal*, 545, 179356. DOI: 10.1016/j.cej.2026.179356.

[33] Mgxadeni, N., Kabane, B., Bahadur, I., Varma, R.S., Singh, S.K. (2023). Deep eutectic solvents as sustainable solvents for industrial separation problems: A recent update. *Journal of Ionic Liquids*, 3(2), 100065. DOI: 10.1016/j.jil.2023.100065.

[34] Jiang, S., Zeng, Y., Zhang, Y., He, Y.-C. (2026). Selective fractionation and enhanced cellulose accessibility of corn Stover using a cetyltrimethylammonium bromide/ethylene glycol/tartaric acid ternary deep eutectic solvent. *Int. J. Biol. Macromol.*, 154045. DOI: 10.1016/j.ijbiomac.2026.154045.

[35] Sanjeeta, Singh, A., Kavirajwar, J. (2025) Dynamic properties and diverse applications of deep eutectic solvents, *Journal of Ionic Liquids*, 5(1), 100135, Jun. 2025, DOI: 10.1016/j.jil.2025.100135.

[36] Zhu, D., Yin, J., Han, S., Zhang, R., Dai, C., He, J., Li, H., Zhu, W., Li, H., Jiang, W, (2026). Ion−dipole−induced high stability of acidic DESs for efficient extractive and oxidative desulfurization. *Chemical Engineering Journal*, 530, 173485. DOI: 10.1016/j.cej.2026.173485.

[37] Shao, Y., Liu, H., Li, L., Wang, K., Wang, X. (2025). Effect and mechanism of hydrogen bonding on the shape-memory effect of wood hydrothermal response. *Ind. Crops Prod.*, 230, 121115, Aug. 2025, DOI: 10.1016/j.indcrop.2025.121115.

[38] Suopajärvi, T., Sirviö, J.A., Liimatainen, H. (2017). Nanofibrillation of deep eutectic solvent-treated paper and board cellulose pulps. *Carbohydr. Polym.*, 169, 167–175. DOI: 10.1016/j.carbpol.2017.04.009.

[39] Putranto, A.W., Dutta, S., Priananda, W., Illias, H.A., Syafiqoh, Q., Masruchin, N., Wibisono, Y., Suhartini, S., Chua, A.S.M., Ngoh, G,C., (2025). Enhancement of cellulose nanocrystal yield from oil palm empty fruit bunches: A comparative study of binary and ternary deep eutectic solvents with pulsed electric field pretreatment. *Biomass Bioenergy*, 196, 107672. DOI: 10.1016/j.biombioe.2025.107672.

[40] Abbas, A. H., Serikov, G., Zhuniskenov, Y., Serikkali, Nyah, F., Ridzuan, N., Gbonhinbor, J., Agi, A. (2024). Revisiting Troubleshooted Drill Stem Test: Methodological Framework Incorporating Artificial Intelligence. *SPE Nigeria Annual International Conference and Exhibition*, SPE, Aug. 2024. DOI: 10.2118/221608-MS.

[41] Husein, N., Ismail, I., Mani, S.V.S., Ker, W.Z., Boyou, N.V., Ismail, A.S.I., Sulaiman, W.R.W. (2020). Experimental investigation of gas-brine liquid flow in horizontal pipeline. *SN Appl. Sci.*, 2(12), 2184. DOI: 10.1007/s42452-020-03944-z.

[42] Hadjer, D., Larbi, H., Abdelkrim, L. (2024). Effect of Xanthan gum on rheological properties of water - crude oil emulsions. *Brazilian Journal of Technology*, 7(4), e76330. DOI: 10.38152/bjtv7n4-050.

[43] Bader, Q.A., Al-Sharify, Z., Dhabab, J.M., Zaidan, H.K., Rheima, A.M., Athair, D.M., Joseph, T.M., Kianfar, E., (2024). Cellulose nanomaterials in oil and gas industry and bio-manufacture: Current situation and future outlook. *Case Studies in Chemical and Environmental Engineering*, 10, 100993. DOI: 10.1016/j.cscee.2024.100993.

[44] Sharma, V., Wang, J. X., Tsai, M-L., Yadav, A., Dong, C-D., Nargotra, P., Sun, P-P. (2025). Bioprocessing of pineapple leaf waste biomass using an integrated ultrasound-deep eutectic solvent pretreatment approach for improved bioethanol production. *J. Biotechnol.*, 404, 83–93. DOI: 10.1016/j.jbiotec.2025.04.011.

[45] Rodriguez-Quiroz, E.S., Olivares-Xometl, O., Santacruz-Vázquez, V., Santacruz-Vázquez, C., Arellanes-Lozada, P., Rubio-Rosas, E. (2023) Production of Cellulosic Microfibers from Coffee Pulp via Alkaline Treatment, Bleaching and Acid Hydrolysis, *Materials*, 16(24), 7607, Dec. 2023, DOI: 10.3390/ma16247607.

[46] Abutu, D., Yussof, H.W., Nwaichi, P.I., Umunnawuike, C., Nyah, F., Money, B., Agi, A. (2025). Biohydrogen production and storage from depleted hydrocarbon reservoirs: A review of the strategies to improve biohydrogen production for sustainable energy transition. *Next Energy*, 9, 100458. DOI: 10.1016/j.nxener.2025.100458.

[47] Nyah, F., Ridzuan, N., Epelle. E., Aziz. M. A. B. A., Gbonhinbor, J. R., Money, B., Abutu, D., Agi, A. (2026). Cellulose bionanomaterial design for enhanced oil recovery: A review of existing, emerging technologies and future outlook. *Petroleum Research*, 11(2), 641–686. DOI: 10.1016/j.ptlrs.2025.12.002.

[48] Kumar, K.R., Vishnu, N.G.C.S., Uppuluri, K.B., Selvasembian, R. (2025). Integrated formic acid and deep eutectic solvent mediated sustainable synthesis of cellulose nanocrystals from Sterculia foetida shells, *Prep. Biochem. Biotechnol.*, 55(4), 403–416. DOI: 10.1080/10826068.2024.2419873.

[49] Prasetyaningsih, Y., Kusumastuti, Y., Ariyanto, T., Hidayat, M. (2025). Optimization of cellulose yield from oil palm trunks with deep eutectic solvents using response surface methodology. *Green Processing and Synthesis*, 14(1). DOI: 10.1515/gps-2024-0252.

[50] Rutkaite, R., Bendoraitiene, J., Pavuolyte, G., Peciulyte, L., Liudvinaviciute, D., Barvainis, P., Varzinskas, V., (2026). Hemp Seed Hull and Cellulose Acetate Thermoplastic Biocomposites and Their Properties. *Molecules*, 31(9), 1453. DOI: 10.3390/molecules31091453.

[51] Wu, X., Yuan, X., Zhao, J., Ji, D., Guo, H., Yao, W., Li, X., Zhang, L., (2023). Study on the effects of different pectinase/cellulase ratios and pretreatment times on the preparation of nanocellulose by ultrasound-assisted bio-enzyme heat treatment. *RSC Adv.*, 13(8), 5149–5157. DOI: 10.1039/D2RA08172E.

[52] Rasheed, M., Jawaid, M., Parveez, B., Zuriyati, A., Khan, A. (2020). Morphological, chemical and thermal analysis of cellulose nanocrystals extracted from bamboo fibre. *Int. J. Biol. Macromol.*, 160, 183–191. DOI: 10.1016/j.ijbiomac.2020.05.170.

[53] Wang, T., Jiang, Y., Shen, R., Shen, F., Tian, D. (2025). Deep Eutectic Solvents Lignin: Extraction. Handbook of Lignin, Singapore: Springer Nature Singapore, pp. 1–21. DOI: 10.1007/978-981-97-2664-6_67-1.

[54] Li, P., Yang, C., Jiang, Z., Jin, Y., Wu, W. (2023). Lignocellulose pretreatment by deep eutectic solvents and related technologies: A review. *Journal of Bioresources and Bioproducts*, 8(1), 33–44. DOI: 10.1016/j.jobab.2022.11.004.

[55] Stanciu, M.-C., Tanasă, F., Teacă, C.-A. (2025). Crystallinity Changes in Modified Cellulose Substrates Evidenced by Spectral and X-Ray Diffraction Data. *Polysaccharides*, 6(2), 30. DOI: 10.3390/polysaccharides6020030.

[56] Pinto, T.C., Barba, L., Papadogiannakis, C., Garcia, A.K., Caliandro, R., Sabet, S., Valoppi, F. (2026). Unveiling the fate of lipid crystalline structures in engineered emulsions during in vitro digestion. *Food Chem.*, 513, 149077. DOI: 10.1016/j.foodchem.2026.149077.

[57] Nugroho, R.W.N., Tardy, B.L., Eldin, S.M., Ilyas, R.A., Mahardika, M., Masruchin, N. (2023). Controlling the critical parameters of ultrasonication to affect the dispersion state, isolation, and chiral nematic assembly of cellulose nanocrystals. *Ultrason. Sonochem.*, 99, 106581. DOI: 10.1016/j.ultsonch.2023.106581.

[58] Zhu, P., Feng, L., Ding, Z., Bai, X. (2022). Preparation of Spherical Cellulose Nanocrystals from Microcrystalline Cellulose by Mixed Acid Hydrolysis with Different Pretreatment Routes. *Int. J. Mol. Sci.*, 23(18), 10764. DOI: 10.3390/ijms231810764.

[59] Hardiningtyas, S.D., Putra, B.U., Angarra, K.B., Yuniasani, I., Ramadhan, W., Pari, R.F., Uji, Hastuti, N., Indrawan, D.A., Wakabayashi, R., Goto, M., Kamiya, N., (2024). Sustainable Synthesis of Cellulose Nanofibers from Industrial Agar Seaweed Waste Biomass Using Hydrated Deep Eutectic Solvents. *Waste Biomass Valorization*, 15(8), 4899–4913. DOI: 10.1007/s12649-024-02499-z.

[60] Imiete, I.E., Giannini, L., Tadiello, L., Orlandi, M., Zoia, L. (2023). The effect of sulfate half-ester groups on the mechanical performance of cellulose nanocrystal-natural rubber composites. *Cellulose*, 30(14), 8929–8940. DOI: 10.1007/s10570-023-05432-0.

[61] Yin, L., Zhang, S., Zhao, D., Wang, R., Jin, Z., Xu, H. (2026). Deep eutectic solvent-ultrasound synergy for simultaneous extraction-modification of Pyrus pyrifolia peel pectin and cellulose nanocrystals: multifaceted physicochemical and structural characterization. *J. Food Sci. Technol*. DOI: 10.1007/s13197-025-06505-7.

[62] Yeo, C.-E., Sung, H.-J. (2025). Eco-Friendly Production of Lignin-Containing Cellulose Nanofibers from Sugarcane Bagasse Fines via Sequential Thermal Hydrolysis–Deep Eutectic Solvents Pretreatment. *Polymers (Basel)*, 18(1), 85. DOI: 10.3390/polym18010085.

[63] Jančíková, V., Jablonský, M., Szadkowska, D., Szadkowski, J., Gemeiner, P. (2024). DES-like mixtures based on choline chloride and lactic acid for fractionation of hemp fibers. *Journal of Ionic Liquids*, 4(1), 100091. DOI: 10.1016/j.jil.2024.100091.

[64] Lopez-Miranda, J.L., Elizalde-Mata, A., Esparza, R., Estevez, M. (2025). Study of Sargassum spp. as a biosorbent material for the elimination of contaminants dissolved in water. *MRS Adv.*, 10(3), 379–385. DOI: 10.1557/s43580-025-01169-z.

[65] Meraj, A., Jawaid, M., Karim, Z., Fouad, H. (2025). Preparation of cellulose nanocrystals extracted from kenaf fiber with natural deep eutectic solvent. *Biomass Convers. Biorefin.*, 15(18), 25351–25358. DOI: 10.1007/s13399-025-06850-9.

[66] Rasoolzadeh, N., Nikzad, M., Mohammadi, M., Bakhshi, H., Amini, G., Koupaie, E.H. (2025). Optimization of cellulose nanocrystal isolation from sorghum bicolor stem using deep eutectic solvents: a response surface methodology approach. *Biomass Convers. Biorefin.*, 5(10), 16189–16212. DOI: 10.1007/s13399-024-06410-7.

[67] Zhang, H., Wu, R., Chen, X., Ni, S., Xu, C., Fu, Y., Qin, M., Zhang, Y., (2025). High-efficient fractionation of poplar chips by ternary deep eutectic solvents system for elevating enzymatic hydrolysis. *Ind. Crops Prod.*, 225, 120489. DOI: 10.1016/j.indcrop.2025.120489.

[68] Karimian, D., Anzuoni, V., Smania, Z., Orian, L., Gross, S., Carraro, M. (2025). Enhanced Nanocellulose Production from Cotton and Textile Waste Using Binary and Ternary Natural Deep Eutectic Solvents. *Adv. Sustain. Syst.*, 9(1). DOI: 10.1002/adsu.202400525.

[69] Yong, W.S., Yong, C.S.C., Yeu, Y.L., Thangavelu, S.K., Chai, A.B., Chung, P.P. (2026). Valorization of sago hampas: extraction of microcrystalline cellulose and its role in enhancing bio-composite properties. *Cellulose*, 33(5), 2857–2885, Mar. 2026, DOI: 10.1007/s10570-026-07010-6.

[70] Zhang, J., Huo, H., Zhang, L., Yang, Y., Li, H., Ren, Y., Zhang, Z. (2022). Effect of High-Temperature Hydrothermal Treatment on the Cellulose Derived from the Buxus Plant. *Polymers (Basel)*, 14(10), 2053. DOI: 10.3390/polym14102053.

[71] Gabriel, T., Wondu, K., Dilebo, J. (2021). Valorization of khat (Catha edulis) waste for the production of cellulose fibers and nanocrystals. *PLoS One*, 16(2), e0246794. DOI: 10.1371/journal.pone.0246794.

[72] Koistinen, A., Vuorinen, T., Maloney, T. (2025). The effect of alkaline pre-treatment on cellulose pulp fiber dissolution. *Carbohydrate Polymer Technologies and Applications*, 11, 100978. DOI: 10.1016/j.carpta.2025.100978.

[73] Nyah, F., Ridzuan, N., Aziz, M.A.B.A., Gbonhinbor, J.R., Nwaichi, P.I., Umunnawuike, C., Abutu, D., Agi, A. (2026). Deep Eutectic Solvents-Derived Functionalized Cellulose Nanoparticles for Interfacial and Wettability Control in Enhanced Oil Recovery. *SPE Nigeria Annual International Conference and Exhibition*, SPE, Aug. 2026. DOI: 10.2118/234812-MS.

[74] Ramli, N.A.N., Sam, S.T., Yaakub, A.R.W., Abdullah, M.F. (2024). Isolation of Cellulose Nanocrystals from Rice Husk using Natural Deep Eutectic Solvent, *International Journal of Biomass Utilization and Sustainable Energy (IJBUSE)*, 1, Sep. 2024, DOI: 10.58915/ijbuse.v1.2024.1081.

[75] Rasoolzadeh, N., Nikzad, M., Mohammadi, M., Bakhshi, H., Amini, G., Koupaie, E.H. (2025). Optimization of cellulose nanocrystal isolation from sorghum bicolor stem using deep eutectic solvents: a response surface methodology approach. *Biomass Convers. Biorefin.*, 15(10), 16189–16212. DOI: 10.1007/s13399-024-06410-7.

[76] Beyan, S.M., Amibo, T.A., Prabhu, S.V., Ayalew, A.G. (2021). Production of Nanocellulose Crystal Derived from Enset Fiber Using Acid Hydrolysis Coupled with Ultrasonication, Isolation, Statistical Modeling, Optimization, and Characterizations. *J. Nanomater.*, 2021, 1–12. DOI: 10.1155/2021/7492532.

[77] Li, J., Wang, Z., Wang, P., Tian, J., Liu, T., Guo, J., Zhu, W., Khan, M.R., Xiao, H., Song, J. (2024). On rheological properties of disc-shaped cellulose nanocrystals. *Carbohydr. Polym.*, 330, 121764. DOI: 10.1016/j.carbpol.2023.121764.

[78] Nyah, F., Ridzuan, N., Aziz. M.A.B.A., Gbonhinbor, J.R., Money, B., Nwaichi, P.I., Umunnawuike, C., Abutu, D., Agi, A. (2025) Cutting-Edge Strategies for Flow Assurance and Multiphase Flow Management in Modern Oil and Gas Operations. *SPE Nigeria Annual International Conference and Exhibition*, SPE. Aug. 2025. DOI: 10.2118/228644-MS.

[79] Rana, A.K., Thakur, M.K., Gupta, V.K., Thakur, V.K. (2024). Exploring the role of nanocellulose as potential sustainable material for enhanced oil recovery: New paradigm for a circular economy. *Process Safety and Environmental Protection*, 183, 1198–1222. DOI: 10.1016/j.psep.2024.01.085.

[80] Money, B., Modather, R.H., Abutu, D., Ismail, N., Agi, A., Nyah, F., Mahat, S.Q.A. (2025). A review on advancing clay-based geopolymers for high-temperature oil well cements: Mechanisms, durability, and applications. *Petroleum Research*. DOI: 10.1016/j.ptlrs.2025.08.005.

[81] Moud, A.A. (2023). CNC Gel Rheology Meets Mechanical Characteristics, in *Advances in Rheology of Materials*, IntechOpen, 2023. DOI: 10.5772/intechopen.106231.

[82] Tatli, B., Rousseau, A.R., Xing, W., Hirsch, M., Cranston, E.D., Abitbol, T. (2026). From Brittle to Flexible: Influence of Glucose-Based Additives on Cellulose Nanocrystal Self-Assembly in Suspension and Dried Photonic Films. *Adv. Opt. Mater.*, 14(6). DOI: 10.1002/adom.202503120.

[83] Pinto, E.A., Dávila, J.L., d'Ávila, M.A. (2019). Rheological studies on nanocrystalline cellulose/alginate suspensions. *J. Mol. Liq.*, 277, 418–423, Mar. 2019, DOI: 10.1016/j.molliq.2018.12.091.

[84] Money, B., Mahat, S.Q.A.B., Melia, A., Gbadamosi, A., Oseh, J., Junin, r., Modather, R.H., Umunnawuike, C., Nyah, F., David, A., Nwaichi, P.I, Agi, A. (2025). Appraising the Impact of Activated Clay Geopolymer as a Sustainable Geopolymer Cement for Oilwell Applications. *SPE Nigeria Annual International Conference and Exhibition*, SPE, Aug. 2025. DOI: 10.2118/228642-MS.

[85] Nwaichi, P.I., Ridzuan, N., Nwaichi, E.O., Umunnawuike, C., Abutu, D., Nyah, F., Money, B., Agi, A. (2025). Advances in oilwell cement retarders: a bibliometric and systematic review of mechanisms, challenges, emerging trends, and future directions. *Discover Concrete and Cement*, 1(1), 8. DOI: 10.1007/s44416-025-00008-6.

[86] Abbas, A.H., Serikov, G., Zhuniskenov, Y., Serikkali, Nyah, F., Ridzuan, N., Gbonhinbor, J., Agi, A. (2024). Navigating the Future: A Numerical Study of Natural Polymers and CO2 in Offshore Applications. *SPE Nigeria Annual International Conference and Exhibition*, SPE, Aug. 2024. DOI: 10.2118/221614-MS.

[87] You, L., Marcolini, B., Bour, J., Grysan, P., Fleming, Y., Fischer, P., Soukoulis, C., (2025). Physicochemical, morphological, and rheological properties of cellulose nanofibrils produced via ultra-high-pressure homogenization. *Carbohydrate Polymer Technologies and Applications*, 9, 100635. DOI: 10.1016/j.carpta.2024.100635.

[88] Wenhao, Z. (2021). Influence of Temperature and Concentration on Viscosity of Complex Fluids, *J. Phys. Conf. Ser.*, 1965(1), 012064. DOI: 10.1088/1742-6596/1965/1/012064.

[89] Altay, B. N., Aksoy, B., Atkinson, J., Lewis, C. L., Diaz-Acosta, C., Francis, R. (2025). Flow dynamics of agricultural waste nanofibers: shear, temperature, and oscillatory insights. *Cellulose*, 32(5), 3077–3094. DOI: 10.1007/s10570-025-06444-8.

[90] Shim, Y.H., Kong, T.Y., Kim, S.Y. (2025). Reversible Control of Rheological Properties in Microgel Composites via Nanoparticle Aggregation. *ACS Appl. Mater. Interfaces*, 17(27), 39616–39627. DOI: 10.1021/acsami.5c06287.

[91] Zhao, Y., Zhang, F., Chen, M., Liu, F., Zheng, B., Miao, W., Gao, H., Zhou, R. (2024). Cellulose nanofibrils-stabilized food-grade Pickering emulsions: Clarifying surface charge's contribution and advancing stabilization mechanism understanding. *Food Hydrocoll.*, 152, 109920. DOI: 10.1016/j.foodhyd.2024.109920.

[92] Liu, E., Meng, H., Zhang, H., Liang, H., Wu, Z. (2024). Nanocellulose, a Renewable Biobased Functional/Reinforcement Additive for Composite Coating Materials: A Review. *ACS Appl. Polym. Mater.*, 6(1), 28–48. DOI: 10.1021/acsapm.3c02088.

[93] Fahma, F., Febiyanti, I., Lisdayana, N., Arnata, I.W., Sartika, D. (2021). Nanocellulose as a new sustainable material for various applications: a review. *Archives of Materials Science and Engineering*, 2(109), 49–64. DOI: 10.5604/01.3001.0015.2624.

[94] Zhang, Q., Ding, Z., Wang, X., Huang, J. (2026). Unveiling Nanocellulose from the Perspective of Morphological Engineering. *Molecules*, 31(16), 2743. DOI: 10.3390/molecules31162743.

[95] Abutu, D., Aderemi, B.O., Ameh, A.O., Yussof, H.W., Gbonhinbor, J., Money, B., Nyah, F., Umunnawuike, C., Nwaichi, P.I., Agi, A. (2025). Optimization of Ethanol Fermentation in a Bubble Column Bioreactor Using Response Surface Methodology with Ferric Oxide Nanoparticle-Modified Supports. *SPE Nigeria Annual International Conference and Exhibition*, SPE, Aug. 2025. DOI: 10.2118/228638-MS.

[96] Muhammed, A.A., Omotosho, Y.A., Aliu, H.O., Adeleke, A.T. (2026). Interfacial tension reduction at crude oil contact with brine-based alumina nanofluid: Experimental and statistical evaluation. *Progress in Engineering Science*, 3(1), 100247. DOI: 10.1016/j.pes.2026.100247.

[97] Deng, X., Patil, S., Al Shehri, D., Kamal, M.S., Shakil, S.M., Zhou, X., Mahmoud, M., Al Shalabi, E.W., Hassan, A. (2023). IFT Reduction Negatively Impacts Oil Recovery When Wettability Alteration Happens. *Gas & Oil Technology Showcase and Conference*, SPE, Mar. 2023. DOI: 10.2118/214178-MS.

[98] Pinto, N O.F., Bourbon, A.I., Martins, D., Pereira, A., Cerqueira, M.A., Pastrana, L., Gama, M., Azeredo, H.M.C., Rosa, M.F. (2024). Bacterial cellulose nanocrystals or nanofibrils as Pickering stabilizers in low-oil emulsions: A comparative study. *Food Hydrocoll.*, 157, 110427, Dec. 2024, DOI: 10.1016/j.foodhyd.2024.110427.

[99] Hansini, A.M.P., Galpaya, G.D.C.P., Gunasena, M.D.K.M., Abeysundara, P.M., Kirthika, V., Bhagya, L., Gunawardana, H.D.C.N., Koswattage, K.R. (2025). From Nature to Innovation: Advances in Nanocellulose Extraction and Its Multifunctional Applications. *Molecules*, 30(13), 2670. DOI: 10.3390/molecules30132670.

[100] Dubey, S., Majumder, S.K. (2026). Synergistic Application of a Plant-Derived Surfactant and CO2 Foam for Enhanced Oil Recovery: Linking Interfacial Phenomena to Core-Scale Performance. *Energy & Fuels*, 40(21), 11397–11418, May 2026, DOI: 10.1021/acs.energyfuels.6c00630.

[101] Wang, C., Jin, G., Wang, W., Zhao, C., Wang, S., Zhao, Y., Ni, J. (2026). Nanomaterials Driving Technological Advancements in Enhanced Oil Recovery from Low-Permeability Tight Oil Reservoirs: Opportunities and Challenges. *Nanomaterials*, 16(8), 464. DOI: 10.3390/nano16080464.

[102] Ebrahimi, M., Ghalenavi, H., Schaffie, M., Ranjbar, M., Hemmati-Sarapardeh, A. (2025). Experimental investigation of wettability alteration in sandstone rock by nanoparticles, gelatin biopolymer, salt ions, and synthesized Fe3O4/gelatin nanocomposite for EOR applications. *Sci. Rep.*, 15(1), 33260. DOI: 10.1038/s41598-025-18591-w.

[103] Mumbere, W., Sagala, F., Gupta, U., Bbosa, D. (2025). Reservoir Potential Unlocked: Synergies Between Low-Salinity Water Flooding, Nanoparticles and Surfactants in Enhanced Oil Recovery─A Review. *ACS Omega*, 10(29), 31216–31261. DOI: 10.1021/acsomega.5c02533.

[104] Al-Musawi, S., Rashidi, F., Amjad-Iranagh, S. (2025). Novel insights into electrical double layers in carbonate reservoirs under low-salinity water injection using molecular dynamics simulation. *Sci. Rep.*, 15(1), 31061. DOI: 10.1038/s41598-025-14647-z.

[105] Song, C., Jang, H., Lee, J. (2023). Synthesis and dispersion stability of seawater-based nano-smart water for application in high-temperature and high-salinity conditions. Colloids Surf. A Physicochem. *Eng. Asp.*, 674, 131910. DOI: 10.1016/j.colsurfa.2023.131910.

[106] Maiki, E.P., Sun, R., Ren, S., AlRassas, A.M., Huang, Y. (2023). Investigating the low salinity effect in a sandstone reservoir through electro-kinetic potential analysis. *Chem. Phys.*, 574, 112028. DOI: 10.1016/j.chemphys.2023.112028.

[107] Nyah, F., Ridzuan, N., Nwaichi, P.I., Umunnawuike, C., Agi, A. (2024). Comprehensive review on the role of salinity on oil recovery mechanisms during chemical flooding. *J. Mol. Liq.*, 415, 126308. DOI: 10.1016/j.molliq.2024.126308.

[108] Abutu, D., Yussof, H.W., Nwaichi, P.I., Umunnawuike, C., Nyah, F., Money, B., Agi, A. (2026). Utilizing depleted oil reservoirs for in-situ biohydrogen production: addressing knowledge gaps, sustainable pathways and future research directions. *Fuel*, 406, 136710. DOI: 10.1016/j.fuel.2025.136710.

[109] Ke, C., Yuan, B., Li, Y., Zhang, W., Tian, J., Dai, C. (2024). Wettability Alteration Induced by Nanoparticle Nonuniform Adsorption and its Impact on Water–Oil Relative Permeability in Heterogeneous Porous Media. *Energy & Fuels*, 38(17), 16133–16148. DOI: 10.1021/acs.energyfuels.4c02944.

[110] Mondal, M.C., Uddin, H.M.W., Progoti, Q. R.M., Tushar, M.A.-N., Dutta, A., Saif, T., Malitha, S.B. (2026). Enhanced oil recovery via metal oxide nanoparticles: A review of recent advancements, core mechanisms, and future outlook. *Next Materials*, 12, 102004, Jul. 2026, DOI: 10.1016/j.nxmate.2026.102004.

[111] Tangparitkul, S., Sukee, A., Jiang, J., Harbottle, D. (2024). Crude oil displacement enhanced by interfacially active nanoparticles and their coupling effect with low-salinity brines. *J. Mol. Liq.*, 408, 125362. DOI: 10.1016/j.molliq.2024.125362.

[112] Manimaran, M., Norizan, M.N., Kassim, M.H.M., Adam, M.R., Abdullah, N., Norrrahim, M.N.F. (2025). Critical review on the stability and thermal conductivity of water-based hybrid nanofluids for heat transfer applications. *RSC Adv.*, 15(18), 14088–14125. DOI: 10.1039/D5RA00844A.

[113] Nyah, F., Ridzuan, N., Aziz. M.A.B.A., Gbonhinbor, J.R., Nwaichi, P.I., Umunnawuike, C., Abutu, D., Agi, A. (2026). Evaluation of Cellulose Nanoparticles Synthesized from Paper Waste as High-Temperature, High-Salinity Nanofluid Agents for Enhanced Oil Recovery. *SPE Nigeria Annual International Conference and Exhibition*, SPE. DOI: 10.2118/234813-MS.

[114] Abutu, D., Nwaichi, P.I., Umunnawuike, C., Nyah, F., Money, B., Yussof, H.W., Agi, A. (2025). Numerical simulation of microbial biohydrogen production under high-pressure, high-temperature conditions for enhanced recovery from depleted reservoirs. *Petroleum Research*. 11(1), 206–216. DOI: 10.1016/j.ptlrs.2025.07.006.

[115] Kandiel, Y.E., Attia, G.M., Metwalli, F.I., Khalaf, R.E., Mahmoud, O. (2025). Nanoparticles in enhanced oil recovery: state-of-the-art review. *J. Pet. Explor. Prod. Technol.*, 15(4), 66. DOI: 10.1007/s13202-025-01965-1.

[116] Khormali, A., Ahmadi, S. (2026). Hybrid nano-chemical enhanced oil recovery processes in oil reservoirs: A critical review. *Results in Engineering*, 32, 112077. DOI: 10.1016/j.rineng.2026.112077.